Physical Observations of Icy Minor Bodies in the Outer Solar System

SEKIGUCHI, Tomohiko
Graduate University for Advanced Studies, 181-8588 Mitaka, Tokyo

September 30, 2001

Abstract

Icy minor bodies in the outer solar system like TNOs (Trans-Neptunian Objects), Centaurs, cometary nuclei and unusual asteroids are thought to be candidates of planetesimal aggregate bodies in the formation theory of the solar system. Therefore, studies of the physical properties of these objects provide clues to the initial conditions for the solar system. However, their physical properties are still poorly known even the most basic parameters like size and albedo because of their extreme faintness. Typical brightness of TNOs in V-band is fainter than 21 magnitude which makes the use of the largest telescopes an indispensable requirement.

Observations were carried out to reveal the characteristics of these faint objects using the largest telescopes. Photometric and low dispersion spectroscopic observations of 16 TNOs and 1 Centaurs in optical and near-IR wavelength were performed for the purpose of colour taxonomical study as the first approach. On the contrary to former studies, absolute magnitude of TNOs and Centaurs shows no significant correlation with the $(V - I)$ colour. Our new measurements of their colours showed no clear bi-modality and continuous diversity from solar to reddened colour of their surface. The surface of TNOs and Centaurs can be modified by resurfacing process of the intrinsic cometary activity. Bi-colour lightcurve observations in high spatial resolution mode, together with deep imaging were performed in order to confirm a cometary activity of TNO 1996 TO_{66}. The inhomogeneous $(V - R)$ colour variation of TNO over one rotation was obtained. It supports the existence of TNO's patchy surface assumption like Pluto's spotted surface. However, cometary coma was not detected down to 29 mag/sq.arcsec. As a next step toward the physical studies of these objects, the determination method of the most basic parameters, size and albedo, and the observing feasibility for the outer minor bodies are discussed. As a trial case, the MUSES-C spacecraft mission target, NEA 1998 SF_{36} was analyzed from thermal observations in mid-IR (N-band). The derived radius and albedo of were 178 (+13/-14) m and 0.29 (+0.05/-0.04), respectively. Finally, the capability of adoption to the faint objects such like TNOs and Centaurs are presented with the possible future facilities.

Contents

List of Figures

List of Tables

Chapter 1

Introduction – Remnants of the Early Solar System

1.1 Icy Minor Bodies in the Outer Solar System Trans-Neptunian Objects and Centaurs

The formation theory of the solar system showed that the planetesimals, as starting objects of proto planet formation, were formed due to fragmentation of the dust layer in the proto planetary disk (Hayashi et al. 1985). In the inner region of the disk, the rocky planetesimals which, consist of condensed materials at relatively high temperature, formed. Then they accumulate through mutual collisions and grew finally into the Earth-type proto planets. In the outer region, the icy planetesimals which were composed of volatile ices and dust, grow into the core of the giant planets. However, it takes too long to form planets beyond Neptune region. Planetesimal remnants or planetesimal aggregates which failed to grow into the proto planets may still remain in the region beyond the Neptune. The early hypotheses of the small objects belt beyond the orbit of Neptune were proposed in 40's and 50's (Edgeworth, 1943, 1949 and Kuiper, 1951).

The first discovery of such an object which orbits the sun beyond Neptune was accomplished by Jewitt and Luu (1993), and with the subsequent detections of more than 400 objects beyond the orbit of Neptune (Trans-Neptunian Objects; hereafter, TNOs) within the last decade, a new category of solar system bodies was established. The TNOs are also called Edgeworth-Kuiper Belt objects, EKBOs, since they are found in the region hypothesized by Edgeworth and Kuiper.

On the other side, similar minor bodies were found as well in the giant planets region; from Jupiter orbit (a=5.2 AU) to Neptune orbit (a=30 AU). They are called Centaurs named after Chiron who was one of the Centaurs, the son of Saturn, and grandson of Uranus in the mythology. Its perihelion is close to the Saturn's orbit, while its aphelion is around the Uranus' orbit (see Table 1.1). The Centaur objects are believed to be scattered TNOs which migrated recently toward the Sun by gravitational interaction with the giant planets (Levison and Duncan, 1997), because the objects in this region are perturbed and are scattered by giant planets. During their temporal resident in the giant planets region, Centaurs suffer from the gravitational scattering by giants. Some parts are scattered away form the planetary region and then some of them play a roll of the formation of Oort cloud (Dones et al. 2000). If the others are scattered into the inner region, they might be very brighter and observable as short period comets (hereafter, SPCs) due to the substantial sublimation of H_2O ice. On the other hand, a part of extinct comets which have exhausted the volatile ice on their surface can be observed as unusual asteroids. A recent analysis of size distribution of comets further supports this evolution track: Meech (2001, priv. comm.) showed that the observed radii are not following a power law as it would be expected if the short-period comets were directly injected in the inner solar system by a collision process.

Since the TNOs and Centaurs never came really close to the Sun, they are considered to be objects which are physico-chemically unaltered population of the solar system bodies. In this respect, they may be even more pristine than SPCs which show obvious activities. Therefore, studies of the physical properties of icy minor bodies, especially TNOs and Centaurs, can provide clues to the initial conditions of

Table 1.1: Dynamical Class of Solar System Minor Bodies

Dynamical Class	Region	Object†	$a^{\ddagger}$ [AU]	In This Paper
Trans-Neptunian Objects	beyond Neptune	**1996 TO_{66}**	43.5	section 2-1, 2-2
Centaurs	Neptune – Jupiter	**Chiron / 1998 TF_{35}**	13.7	section 2-1
Main Belt Asteroids	Jupiter – Mars	**Ceres**	2.77	—
Near-Earth Asteroids	Near Earth	**1998 SF_{36}**	1.32	section 2-3

Note: † : example object or analyzed object in this paper ‡ : semi major axis

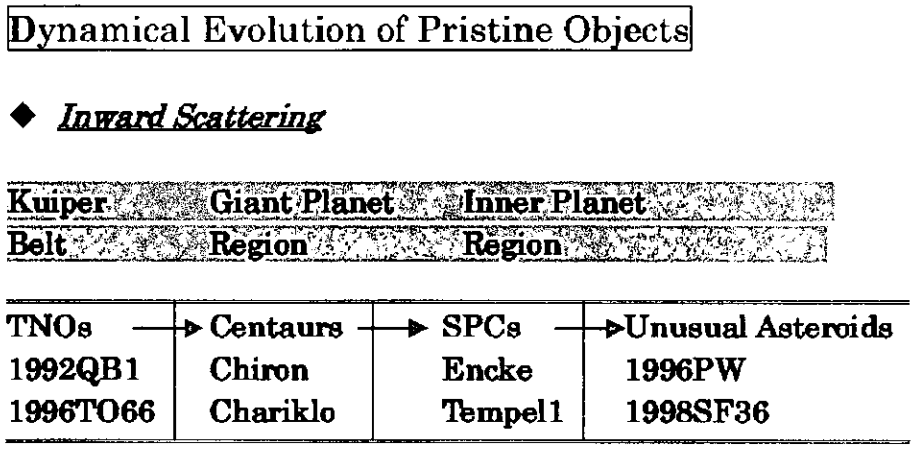

Figure 1.1: Dynamical Evolution Scheme of Icy Minor Bodies

the solar system.

1.2 Physical Properties of Icy Minor Bodies

The physical properties of such objects should be important in aspects mentioned above. However, their characteristics are still poorly known even for the most basic parameters like size and albedo because of their faintness. Typical brightness of TNOs is fainter than 21 magnitude in V-band. Such an extreme faintness makes the utilizations of the largest telescopes indispensable.

In pursuit of this study execution, the author belonged to the European Southern Observatory (ESO), Chile, more than 2 years, awarded by ESO through the ESO Ph.D studentship programme, and performed his work from the following point of view.

- **Attempt toward Classification of Icy Minor Bodies:**

  As a pilot study to know their characteristics, Tegler and Romanishin (1998) performed BVR photometry of 11 TNOs and 5 Centaurs for the purpose of colour classifications. They reported the presence of two distinct populations of their colours. One consists of objects whose surface colours are only slightly redder than the solar colour, while the other consists of the reddest objects known in the solar system. However, 16 data points may not be enough to establish a classification. Barucci et al. (1999b) reported colour diversity from solar analogue colour to red colour by optical spectroscopy of 5 Centaurs, even they are in the same dynamical class. Recent observations confirmed that the colour of a Centaur object, Chiron was similar to the sun, while the colour of a Centaur, Pholus was very red (Davies et al. 2000, Barucci et al. 2000, Trujillo et al. 2000). Nevertheless, further observational works are still strongly needed to characterize their surface colours and to confirm previous results. The BVRI photometory of 16 TNOs and 1 Centaur, and 5 TNOs' spectra were obtained by our observing team at ESO Chile. The increase of number of measured colours revealed the diversity of their surface colour (in section 2.2).

- **Surface albedo variations through Cometary Activity:**

  All icy bodies may have suffered from their surface reddening over the age of the solar system. Laboratory experiments showed that the icy surface was modified by the high energy particle and the solar UV irradiation (Khare *et al.*, 1984, Sagan *et al.* 1984). The carbonized compounds of the surface volatiles which were transmuted into more complex, polymerized material by irradiation, attribute to reddening. Since the fresh material shows less red colour, the transport mechanism of the fresh ice under their surface is required to explain the non-red colour of TNOs and Centaurs. Theoretical model suggested TNOs have suffered from collisional erosion by dust and small debris (Stern, 1995, Stern, 1996). Luu and Jewitt (1996b) tried to explain the colour diversity with collision-vs-reddening model. On the other hand, Luu and Jewitt (1996a) suggested the hypothesis that fall-back debris by cometary activity may have coated the surface of Centaurs. Non red spectrum of Chiron can be explained with resurfacing process through its cometary activity. After Chiron shows its activity and cometary coma (Meech, 1990), only Chiron was registered as a numbered short period comet among Centaur objects. The absorption bands of volatile ice (H_2O) were found in two Centaurs (Chiron; Luu et al. 2000, Chariklo; Cruikshank et al. 1998).

  Recently, Hainaut *et al.* (2000) reported the lightcurve change of TNO 1996 TO_{66} between 2 years and proposed a hypothesis of cometary activity of the TNO. The spectrum of 1996 TO_{66} also show non red colour which requires resurfacing process. Moreover the absorption features of volatile ice (H_2O) of the TNO were found from this TNO in the near-IR (Brown et al. 1999, Noll et al. 2000), although H_2O ice hardly sublimates at the temperature in the outer solar system. These results suggests the possible cometary activity of this TNO. The time-resolved photometry of 1996 TO_{66} was performed to find out any evidence of cometary activity by two-colour imaging. The existence of a patchy part on the surface, which is possibly made by the cometary activity, was suggested although no coma was detected (section 2.2).

- **Determination of Size and Albedo:**

  The geometric albedo and size are the most basic parameters on the physical properties of icy minor bodies. However, they are only poorly known since the thermal radiations of the outer solar system objects are in very little due to the low temperature and long distance. Most of current studies to obtain the physical properties are to measure their reflected light of the solar radiation in optical and near-IR. On the other hand, the icy minor bodies emit their blackbody radiation in mid–far IR range. The method to obtain their size and albedo is examined with a bright unusual asteroid which can be a rocky minor body but may be a relative of icy minor bodies in the outer solar system. While a part of unusual asteroids might originate as the fragments of main-belt asteroids (Rabinowitz, 1997), a part of them might be extinct comets which have exhausted the volatile ice on their surface (Weissman & Levison, 1997) As a trial case for bright target, NEA 1998 SF_{36} which is the MUSES-C spacecraft mission target, was analyzed from thermal observations in mid-IR (N-band).

  The method and the observing feasibility for the outer minor bodies are discussed. The measurements of thermal emission with the future instrument like VLT and ALMA allow us to obtain the real size of icy minor bodies. It will give an important condition on the growth time of planetesimals for the planet formation theory.

1.3 Questions and Approaches

Key questions to be answered for the icy minor bodies are:

1. Is it possible to establish a taxonomical classification with colour observations as the first step for the determination of their chemical compositions?
2. What is the reason for the colour diversity from solar to red? Are TNOS active?
3. What are the diameters? How can the size distribution be obtained without an assumption of surface albedo?

Table 1.2: List of used telescopes and instruments

Purpose	Telescope	Instrument	Wavelength
1 & 2	VLT 8.2m (ESO)	FORS	optical
1	Calar Alto 3.5m	MOSCA	optical
1	NTT 3.5m (ESO)	SOFI	Near-IR
3	ESO 3.6m (ESO)	TIMMI2	Mid-IR

To solve and/or to approach these questions, the studies and methods below are described in this paper.

(1) Optical and near-IR photometory and spectroscopy: the increasing of the number of colour data and acquisition of the colour gradients allow us to establish a classification or a characterization.

(2) Optical Photometry: the high spatial resolution imaging is the best method to search cometary activity. the 2 colours photometry is the first step to investigate the variations of surface colours.

(3) Thermal observations: mid-IR and sub-millimeter observation allow us to determine the size and albedo simultaneously.

Chapter 2

Photometric Studies of Icy Minor Bodies

2.1 Surface Characterization of TNOs and Centaurs

Optical and Near-IR Colours

In this section, visible (BVRI) and near-IR (JHK_s) broadband photometry and visible low-dispersion spectroscopy of Trans-Neptunian Objects (TNOs) and Centaurs are presented in order to characterize their reflectance properties, especially, to examine and confirm the previous results. One is the strong correlation between surface colour and absolute magnitude reported by Luu and Jewitt (1998). The other is the distinct classification proposed by Tegler and Romanishin (1998). No clear global correlation between $V-I$ colour and absolute R filter brightness of our TNO targets is found. The colour-colour diagrams do not suggest a double-peak population of TNOs in B-V vs V-R strongly and suggest continuous reddening in V-R vs R-I and B-V vs R-I.

The knowledge of physical parameters of TNOs and Centaurs suffers from the faintness of the objects which calls for observations with large telescopes on the ground or for observations with the Hubble Space Telescope (HST).

Size estimates exist from coarse single or two colour photometry obtained by the search programs. More accurate multi-colour photometry of about 30 TNOs in the visible wavelength range is published, near-IR colours of TNOs are rarer. 6 Centaurs have visible

and near-IR broadband colours measured. For a more recent compilation of the published photometry data of TNOs and Centaurs see (Barucci et al. 1999a.)

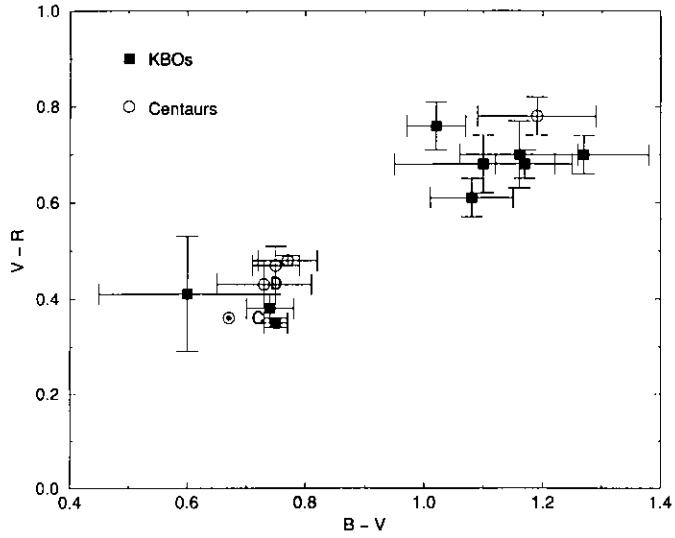

Figure 2.1: Colour-colour diagrams of TNOs and Centaurs (Tegler and Romanishin, 1998).

Obviously, TNOs and Centaurs exhibit different reddening in their broadband colours which may be indicative for different processing of their surfaces. At present, the existence of two TNO groups with distinct colours appears to be controversial (Tegler and Romanishin 1998, Davies et al. 2000, Barucci et al. 2000, Trujillo et al. 2000). Spectra of a handful TNOs are available in literature: while the visible spectra of TNOs (Jewitt&Luu 1998) appear featureless, absorption bands of water ice were found in one TNO in the near-IR (1996TO66; Brown et al. 1999, Noll et al. 2000).

The Centaurs have either neutral or very red colours. Spectroscopy (5 objects published, Barucci 1999b) in the visible and near-IR revealed mostly reflectance spectra, but in one case also CN gas emission (Bus et al. 1991). K band water ice absorptions were also reported (Cruikshank et al.1998).

In the following sections we present photometry (visible and near-IR) of 16 TNOs and 1 Centaur as well as visible spectra of 5 TNOs. The observations are part of a co-ordinated program for the exploration of physico-chemical properties of TNOs and Centaurs, executed.

2.1.1 Observations at ESO VLT, NTT and at Calar Alto

The observations were collected in the visible and near-infrared (near-IR) wavelength ranges during 5 runs between 1998 and early 2000 at the ESO observatories in La Silla and Paranal and at the Calar Alto Observatory in Spain (Table 2.1). In La Silla we used the 3.6m New-Technology-Telescope (NTT) equipped with the near-IR instrument SOFI. At Paranal we used the 8.2m UT1 Telescope of the ESO Very Large Telescope VLT. In 1998 UT1 was equipped with the VLT Test Camera (TC), in 1999 we used the FORS1 instrument. Both the TC and FORS1 work in the visible wavelength range. The Calar Alto data were also collected in the visible wavelength range at the 3.5m telescope using the MOSCA focal reducer. The filters and wavelength ranges used during the various observing runs are listed in Table 2.1. Details on the telescopes and instruments can be found on the web pages of these observatories. The log of the observations is given in Table 2.2 and Table 2.3. It should be noted that, at the ESO telescopes, we used filters from the Bessel system for imaging, while at Calar Alto Johnson-type BVI filters and a special R passband filter with steep cut-off near 750nm were installed. The objects were selected with the goal to contribute new and/or improved broadband colours in the visible and near-IR wavelength range for the taxonomic characterization and classification of TNOs and Centaurs. The spectroscopy part focused on a subset of the objects imaged with broadband filters. The spectra were obtained either immediately before or after the filter imaging of the respective objects.

All images and spectra were taken under photometric conditions. During imaging the telescopes were used in sidereal tracking/auto-guiding mode. During spectroscopy differential tracking/auto-guiding was applied in order to keep the objects on the 1" wide slit. At the VLT all three or four colours (B)VRI of the objects were measured within a short time interval (typically within 20-25min) at least in one night in order to minimize possible brightness variations due to rotation. The 3.5m Calar Alto photometry had longer execution time per object. Therefore, in most cases the sequences of consecutive exposures in RBRVIR filters were used for the sampling of the rotation variability. During near-IR imaging random jitter offsets of the telescope were applied during the filter exposure series.

In addition to the object exposures also photometric and spectrophotometric standard stars, flatfield, arc spectra and bias exposures were taken as needed for the calibrations of the data.

Table 2.1: Telescope and instruments for the TNO/Centaurs observations

Observ. Period	Observatory Tel. + Inst.	Filters Sp.Range (nm)	Imaging Objects Spectroscopy Objects
24-26 Aug 1998	ESO Paranal VLT UT1 + TC	img.: BVRI (Bessel)	img.: 1993RO, 1996TL66, 1996TP66
19-20 March 1999	ESO La Silla 3.6m NTT +SOFI	img: JHK$_s$	img.: 1995HM5, 1997CQ29, 1997CS29
13-15 May 1999	ESO Paranal VLT UT1 + FORS1	img.: VRI (Bessel) spec.: 590-1000	img.: 1994EV3, 1997CQ29, 1998HK151 spec.: 1997CQ29, 1998HK151
2-6/12/1999	ESO Paranal VLT UT1 + FORS1	img.: BVRI (Bessel) spec.: 350-1000	img.: 1992QB1, 1995SM55, 1996RQ20, 1996TO66, 1997CS29 spec.: 1995SM55, 1996TO66, 1997CS29
3-6 Jan. 2000	Calar Alto 3.5m + MOSCA	img.: BVRI (Johnson+special)	img.: 1997CS29, 1998TF35, 1998VG44, 1998WH24, 1998XY95, 1999TC36

Notations: img.: imaging, spec.: spectra in given wavelength range.

2.1.2 Data Processing

In the following subsections the data reduction steps are described separately for imaging photometry in the visible and near-IR as well as for visible spectroscopy.

Visible Imaging Data: TC, FORS1 and MOSCA

TC: since these exposures are part of the VLT UT1 Science Verification (SV) Program, we used the completely reduced images as provided by the SV team (for the reduction steps applied see Giacconi et al. 1999). A small additional work was necessary to identify the TNOs in the reduced images and to obtain the brightness values of the objects in the various filters. This step of the data reduction is described in Hainaut et al. (2000).

FORS1 and MOSCA: the usual CCD "cosmetic" data reduction, i.e. bias subtraction, flat fielding and cosmic ray removal, was at first applied to all the object frames (science objects and standard stars). As bias image, the median of all bias images taken at the beginning and at the end of the nights was used, since no significant changes were found from the frames taken at different times. As flat field images we used the average of several twilight sky images, normalized to 1. To reduce the cosmic ray signature we filtered the bias and flat field corrected object images with a 3×3 pixels wide median filter. The difference between unfiltered and filtered images showed that no other small-scale structures, but only cosmic ray events were erased from the object images. Sky correction was performed by subtracting a first order polynomial sky approximation computed from the pixel areas containing no stars. The TNOs/Centaurs were then identified by blinking two images recorded at different times. As we observed only objects whose orbit is well known, this ensures proper identification.

Photometry (Data): From the measured magnitude of the standard stars, after the application of the instrumental colour and air mass corrections (for detailed information see the ESO VLT Quality Control web page http://www.eso.org/observing/dfo/quality/), the zero-points for the nights were computed. With these zero-points and with first order measurements of objects' colours, the magnitudes of the TNO (see Table 2.2 and Table 2.3) were obtained applying the quoted colour and air mass corrections. The measurement errors given in these tables are the quadratic combination of the photometric and calibration errors. The resulting magnitudes are in the Bessel filter system as defined in Landolt (1992). Generally, apart from the relatively bright objects, the calibration errors are negligible in comparison with the photometric ones. Regarding the photometric errors the largest source is produced by the sky noise, even in the V band where the sky intensity is at minimum. For that reason, to avoid any possible source of systematic errors, it is important to subtract the sky background correctly and to measure the total counts in the smallest possible aperture. In our case the aperture radius varied from 6 to 10 pixels, depending on the seeing present at the time of the observation (note: the diameter for the photometry was larger – by a factor of about 2 - than the FWHM (full width at half maximum) of the TNO images which is typically taken as a measure for the image quality).

The MOSCA data was processed in the same way as the FORS1 ones except for the following steps: (1) for each colour the extinction values of the site were determined from standard star images taken every night in the same filter at different air masses. (2) the colour coefficients were obtained from the same standard star data using a linear correction term for R-I. This colour transformation took care of the transition of the instrumental colours in the Johnson/special filter set used for the observations into the Bessel filter system needed for the scientific analysis of the results. (3) we applied aperture photometry measurements only. The aperture radius of the measurement series varied between 1 and 4 sigma of the PSF.

Visible Spectroscopic Data

FORS1: basic reduction steps – the raw exposures were first bias subtracted, flat field corrected and cosmic ray filtered. The bias frame was the median of several frames recorded at the beginning and the end of the night. The master flat field was computed as the median of several exposures measured on the illuminated internal screen of FORS1, normalized to one. Since the sharpest intensity variations were in wavelength direction, a median filter of dimensions equal to 1 pixel in the λ-direction and 3 pixels along the slit was used to filter the cosmic rays. It was also checked that almost all and only cosmic rays

Table 2.2: Log and Results of the TNO/Centaur observations.
– ESO NTT and VLT results–

Object Tel.+Inst.	Date (UT)	Exp.Time (sec)	Filter/ Spectrum	Brightness (mag)	Error (mag)
1992QB1	1999 Dec 05.022	300+400	V	23.69	0.08
UT1+FORS1	05.026	300+400	I	22.53	0.07
	05.031	600	B	24.69	0.18
	05.039	400	R	23.09	0.06
1993RO	1998 Aug 24.350	600	V	24.37	0.08
UT1+TC	24.402	600	R	23.63	0.08
	24.460	600	I	23.15	0.08
1994EV3	1999 May 13.989	300	V	23.97	0.13
UT1+FORS1	13.993	300	R	23.68	0.15
	13.997	600	I	22.84	0.13
1995HM5	1999 Mar 20.300	3120	J	22.40	0.29
NTT+SOFI	20.320	2160	H	21.20	0.37
1995SM55	1999 Dec 02.026	300	V	21.22	0.05
UT1+FORS1	02.030	300	I	19.89	0.03
	02.035	300	B	21.22	0.05
	02.041	90	R	20.28	0.03
	02.045	1200	590-1000nm	Fig. 2.2	red only
1996RQ20	1999 Dec 04.031	200+400	R	22.92	0.05
UT1+TC	04.034	300	V	23.60	0.08
	04.038	400	I	22.34	0.08
	04.044	600	B	24.49	0.12
1996TL66	1998 Aug 24.250	600	B	21.81	0.07
UT1+TC	24.260	600	V	21.46	0.06
	24.270	600	R	20.83	0.06
	24.282	600	I	23.46	0.07
1996TO66	1999 Dec 03.020	200	V	21.62	0.03
UT1+FORS1	03.024	200	I	20.91	0.04
	03.027	300	B	22.18	0.06
	03.031	100	R	21.14	0.03
	03.035	2x1200	350-1000nm	Fig. 2.2	blue+red (1)
1996TP66	1998 Aug 24.332	600	B	22.89	0.08
UT1+TC	24.341	600	V	21.86	0.06
	24.353	600	R	21.27	0.06
	24.365	600	I	20.62	0.07
1997CQ29	1999 Mar 20.142	2400	J	21.68	0.18
NTT+SOFI	20.145	1920	H	21.02	0.34
UT1+FORS1	1999 May 13.975	300	V	23.53	0.11
	14.991	2x180	V	23.91	0.11
	14.973	300	R	23.21	0.08
	14.977	600	I	22.59	0.11
	15.007	3600	590-1000nm	Fig. 2.2	red only
1997CS29	1999 Mar 20.060	720	J	20.30	0.10
NTT+SOFI	20.060	1440	H	20.00	0.12
	20.080	1440	K_s	20.10	0.20
UT1+FORS1	1999 Dec 05.300	2x200	R	21.27	0.04
	05.303	400	I	20.73	0.03
	05.309	500	B	22.88	0.06
	05.318	250	V	21.99	0.05
	05.325	1246	350-1000nm	Fig. 2.2	blue+red
3.5m+MOSCA	2000 Jan 04.057	600	V	22.17	0.05
	04.067	2x450	I	20.72	0.05
	04.069	3x600	R	21.39	0.03
	04.092	1200	B	23.20	0.06
1998HK151	1999 May 14.302	300	V	22.12	0.03
UT1+FORS1	15.243	2x300	V	22.06	0.03
	14.310	300	R	21.63	0.03
	14.314	600	I	21.20	0.05
	15.242	600	I	21.21	0.04
	15.258	3600	590-1000nm	Fig. 2.2	red only

Note:All magnitudes apply for the Bessel filter system.

Table 2.3: Log and Results of the TNO/Centaur observations– Calar Alto results

Object Tel.+Inst.	Date (UT)	Exp.Time (sec)	Filter	Brightness (mag)	Error (mag)
1998TF35	2000 Jan 04.978	600	V	22.26	0.05
3.5m+MOSCA	04.998	2x600	R	21.55	0.03
	05.000	2x450	I	20.98	0.09
	05.020	1200	B	23.28	0.10
1998VG44	2000 Jan 05.940	600	V	21.75	0.03
3.5m+MOSCA	05.955	3x600	R	21.14	0.03
	05.977	1500	B	22.68	0.04
	06.004	2x450	I	20.37	0.07
1998WH24	2000 Jan 03.967	1200	B	22.39	0.04
3.5m+MOSCA	03.988	600	V	21.56	0.04
	03.994	2x600	R	20.92	0.02
	04.000	2x450	I	20.53	0.04
1998XY95	2000 Jan 05.061	900	V	23.40	0.12
3.5m+MOSCA	05.071	2x600	R	22.75	0.07
	05.080	3x450	I	21.98	0.14
	05.123	1500	B	24.33	0.20
1999TC36	2000 Jan 04.799	600	B	21.71	0.03
3.5m+MOSCA	04.815	600	V	20.75	0.03
	04.822	2x600	R	20.05	0.02
	04.829	2x450	I	19.47	0.03

Note: In case of multiple exposures within RBRVIR filter sequences the mid exposure time and average filter brightness is given. All magnitudes apply for the Bessel filter system.

were eliminated, by inspecting the difference image between unfiltered and filtered ones.

For the wavelength solution and object signal extraction, the dispersion curve was obtained and the spectra were calibrated in wavelength by using HeAr spectra. At the same time possible geometrical distortion of the lines were also corrected. By integrating over the along-slit extension of the spectral profiles and subtracting the sky lines, one-dimension spectra of the objects were obtained. For this operation particular care was necessary in order to use the minimum possible width of the spectrum for the extraction of the object signal, without loosing signal or introducing possible artificial colour, since the spectra were very weak and the sky contribution high. For the response and flux calibration, spectrophotometric standard star spectra, once corrected for air mass extinction, were used to derive the instrumental response curve. The response was used to obtain the flux calibrated TNO spectra. Finally, all spectra available for a single object were co-added and convolved with the instrumental point spread function (a Gaussian profile with FWHM = 2.5nm). The reflectance curves of the TNOs were obtained by dividing the respective final spectra of an object by the catalogue solar spectrum, flux calibrated, and convolved with the same instrumental point spread function.

In the final spectra (both the flux calibrated and the reflectance ones) the major source of noise is produced by the sky emission lines, some of which amount to more than 10 times the signal of the objects.

Near Infrared Data

SOFI: The standard procedure for infrared data reduction was also applied for the NTT/SOFI infrared observations. First of all, The flat field response for each band was obtained as difference of dome exposures taken with light on and off, normalized to 1. From each observing sequence of the objects a master sky frame was obtained as median of several frames recorded with the telescope pointing always in slightly different positions (jitter images). The reduced frames were computed as difference of a single object frame minus the sky one, divided by the flat field frame. In this way the sky contribution, the bias and the possible telescope background were also subtracted from the resulting frame. Since a single object frame had a typical exposure time of the order of 1 min, the faint TNOs were not easily visible in these images. Therefore, in order to identify the targets, all frames were re-aligned to the computed position of the TNOs using the background stars present in the field and the predicted proper motion of the TNOs. The median of all the aligned images gave an image with the TNO well visible and the background stars dimmed (depending on the TNO proper motion, the length of the exposure and the brightness of the field stars). For infrared photometry, the measurement of the magnitude

of the observed objects was made according to the same procedures used for the FORS1 data. Actually the procedures work much better here, because the background stars were dimmed by the median average.

The measurements of the standard stars followed the same procedure apart that the realignment was done to the stars themselves. By applying colour and air mass correction for La Silla the NTT/SOFI zero points were obtained. Since the emission of the sky in the infrared region is much larger than that in the visible, the greatest error contribution in the measured magnitude was the sky noise.

2.1.3 Results

The filter photometry of the observed TNOs and Centaur as obtained from our images is given in Table 2.2 and Table 2.3. Table 2.1.3 lists the absolute brightness M_R, the equivalent radius and the colours of the objects as derived from the data in Table 2.2 and Table 2.3. It also lists the spectral gradients of the TNOs as obtained from the colours (B-I and V-I) and from spectra (red, blue&red) and provides a type indication from both the orbit and the photometric data.

The reflectivity spectra of the observed TNOs are shown in Figure 2.2. Figure 2.5 shows their V-I colours versus the absolute brightness in the R passband. Colour-colour diagrams of the TNOs and Centaurs are given in Figure 2.6. The reddening gradient statistics of the TNOs and Centaurs is displayed in Figure 2.7. Figures 2.2 and 2.5 show results of our own observations only. Figure 2.6 allows the comparison between our data and the ones found in literature. Figure 2.7, finally, combines all existing data as explained below (see also Table 2.6).

The absolute magnitude M_R of the object is derived from its R filter brightness using the formula for asteroids (adopted by IAU Commission 20; Meeus 1998). For the phase correction factor G a standardized value of 0.15 is applied. The error of M_R is identical with the measurement uncertainty of the R filter brightness. M_R can be considered as a measure of the product "geometric cross-section $\times$ albedo of the object". The equivalent radius of the object is obtained applying the classical formula by Wyckhoff (1982) and assuming an albedo of 0.04. With one exception (1995HM5 for which we have near-IR data only) our absolute magnitude and equivalent radii refer to R filter brightnesses of the objects.

The colour gradients grad(C1,C2) indicate the reddening of the objects and are derived from B-I, V-I and V-J colours. They are given in "percent per 100nm" and can be calculated via formula 2.1:

$$grad(C1,C2) = \frac{10^{0.4\times[(C1_{tno}-C2_{tno})-(C1_{\odot}-C2_{\odot})]}-1}{(\lambda_{C1}-\lambda_{C2})}10^4 \qquad (2.1)$$

where

$C1_{\rm tno}$, $C2_{\rm tno}$: the brightness of the TNO/Centaur in filters C1 and C2

$C1_{\odot}$, $C2_{\odot}$: the filter brightness of the Sun

$\lambda_{C1,C2}$: the central wavelength of the filters C1 and C2.

The corresponding spectral gradients can be measured directly from the reflectance spectra of the objects (using the "reference wavelength" of 600 – 900 nm for the red spectra and 400 – 900 nm if blue and red spectra are available).

Table 2.4: TNO/Centaur absolute brightness, radii, colours and spectral gradients

Object Dyn. Type	M_R Radius [mag]/[km]	B-V δB-V [mag]	V-R δV-R [mag]	R-I δR-I [mag]	V-J δV-J [mag]	J-H δJ-H [mag]	H-K_s δH-K_s [mag]	grad(B-I) grad(V-I) [%/100nm]	grad(spectrum) spectral type [%/100nm]
1992QB1	6.82±0.06	1.00	0.60	0.56	—	—	—	30±10	—
Cubewano	120±3	0.20	0.10	0.09	—	—	—	21±6	very red
1993RO	8.56±0.08	—	0.74	0.48	—	—	—	—	—
Plutino	54±2		0.11	0.11	—	—	—	25±7	very red
1994EV3	7.08±0.15	—	0.26	0.80	—	—	—	—	—
Cubewano	107±8	—	0.20	0.20	—	—	—	16±9	blue outliers
1995HM5	22.39±0.29(1)	—	—	—	—	1.18	—	—	—
Plutino	67±10(1)	—	—	—	—	0.47	—	—	outliers ?, peculiar H-K
1995SM55	4.20±0.03	0.68	0.28	0.39	—	—	—	-1±1	-12±5
Cubewano	404±6	0.06	0.04	0.04	—	—	—	-1±1	bluish
1996RQ20	6.82±0.05	0.89	0.68	0.58	—	—	—	30±8	—
Cubewano	112±3	0.14	0.09	0.09	—	—	—	27±7	very red
1996TL66	5.30±0.06	0.35	0.63	0.37	—	—	—	0±3	—
Scattered	243±7	0.09	0.08	0.09	—	—	—	13±4	neutral to slightly red
1996TO66	4.36±0.03	0.56	0.48	0.23	—	—	—	-2±2	3±3
Cubewano	375±5	0.07	0.04	0.05	—	—	—	1±2	neutral to slightly red
1996TP66	7.05±0.06	1.03	0.58	0.66	—	—	—	36±6	—
Plutino	109±3	0.10	0.08	0.09	—	—	—	26±6	very red
1997CQ29	6.86±0.08	—	0.72	0.61	2.24	0.66	—	—	27±5
Cubewano	109±4	—	0.14	0.14	0.25	—	—	31±13	very red
1997CS29(VLT)	4.76±0.04	0.89	0.72	0.54	1.72	0.31	0.36	30±4	27±3
Cubewano	312±6	0.08	0.06	0.05	0.11	0.16	0.23	27±4	very red
1997CS29 (CA)	4.97±0.03	1.03	0.78	0.54	2.15	—	—	50±6	—
as above	283±4	0.08	0.06	0.06	0.07	—	—	40±5	as above
1998HK151	6.86±0.03	—	0.45	0.42	—	—	—	—	7±3
Plutino	118±2	—	0.04	0.04	—	—	—	7±3	neutral to slightly red
1998TF35	8.60±0.03	1.02	0.71	0.57	2.30	—	—	38±8	—
Centaur	53±1	0.11	0.06	0.09	0.13	-	—	29±6	very red
1998VG44	6.16±0.03	0.93	0.61	0.77	2.31	—	—	39±5	—
Plutino	163±2	0.05	0.04	0.04	0.08	—	—	35±5	very red
1998WH24	4.53±0.02	0.83	0.64	0.39	1.86	—	—	16±2	—
Cubewano	347±3	0.06	0.04	0.04	0.06	—	—	15±3	medium red
1998XY95	6.39±0.07	0.93	0.65	0.77	2.35	—	—	41±16	—
TNO	147±5	0.23	0.14	0.16	0.24	—	—	38±13	very red
1999TC36	4.77±0.02	0.96	0.70	0.58	2.24	—	—	35±2	—
TNO	310±3	0.04	0.04	0.04	0.04	—	—	29±3	very red
Sun		0.67	0.36	0.33	1.08	0.29	0.06		

Notations: VLT = measured at VLT, CA = measured at Calar Alto.
The objects are listed according to designation.

Table 2.1.3 lists for each object:

- the object designation and, if known, the dynamical type (Plutino, Cubewano, Scattered = scattered disk object, Centaur, TNO = unclassified TNO)
- the absolute R filter magnitude M_R (except for 1995HM5 which is based on the J filter brightness).
- the equivalent radius derived from the R filter brightness (except for 1995HM5 which are based on the J filter brightness) for an assumed albedo of 0.04.
- the colours of the objects in a set of cardinal filters (B-V, V-R, R-I, V-J, J-H, H-K_S). The photometric errors of the colours are given in the second line (calculated by standard error propagation from the measurement errors for each filter).
- the colour (B-I and V-I) gradients according to Equation 2.1 as well as the gradient measured in the reflectance spectra (if available).
- the photometric type of the objects classified according to the colour gradient statistics. Bluish: gradient < 0 [%/100nm]; neutral to slightly red: gradient 0–10 [%/100nm]; medium red: gradient 10–25 [%/100nm]; very red: 25–40 [%/100nm]; outliers: anything else.

Reflectance spectra

The reflectance spectra of the 5 TNOs observed (see Figure 2.2) are featureless, i.e. without indications for (neither emission nor absorption) spectral lines or bands intrinsic to the objects. The scatter in the red end of the spectra is due to incomplete subtraction of very bright skylines.

The spectral gradients are very constant over the measured wavelength ranges. However, marginal changes of the spectral slopes exist toward the red end of some spectra possibly indicating less steep reddening of the objects toward the near-IR region. Overall, the spectral gradients agree very well with the photometric ones for all measured objects except 1995SM55 for which the spectrum shows a negative gradient while the photometry gives neutral colours; see also section 2.1.3.

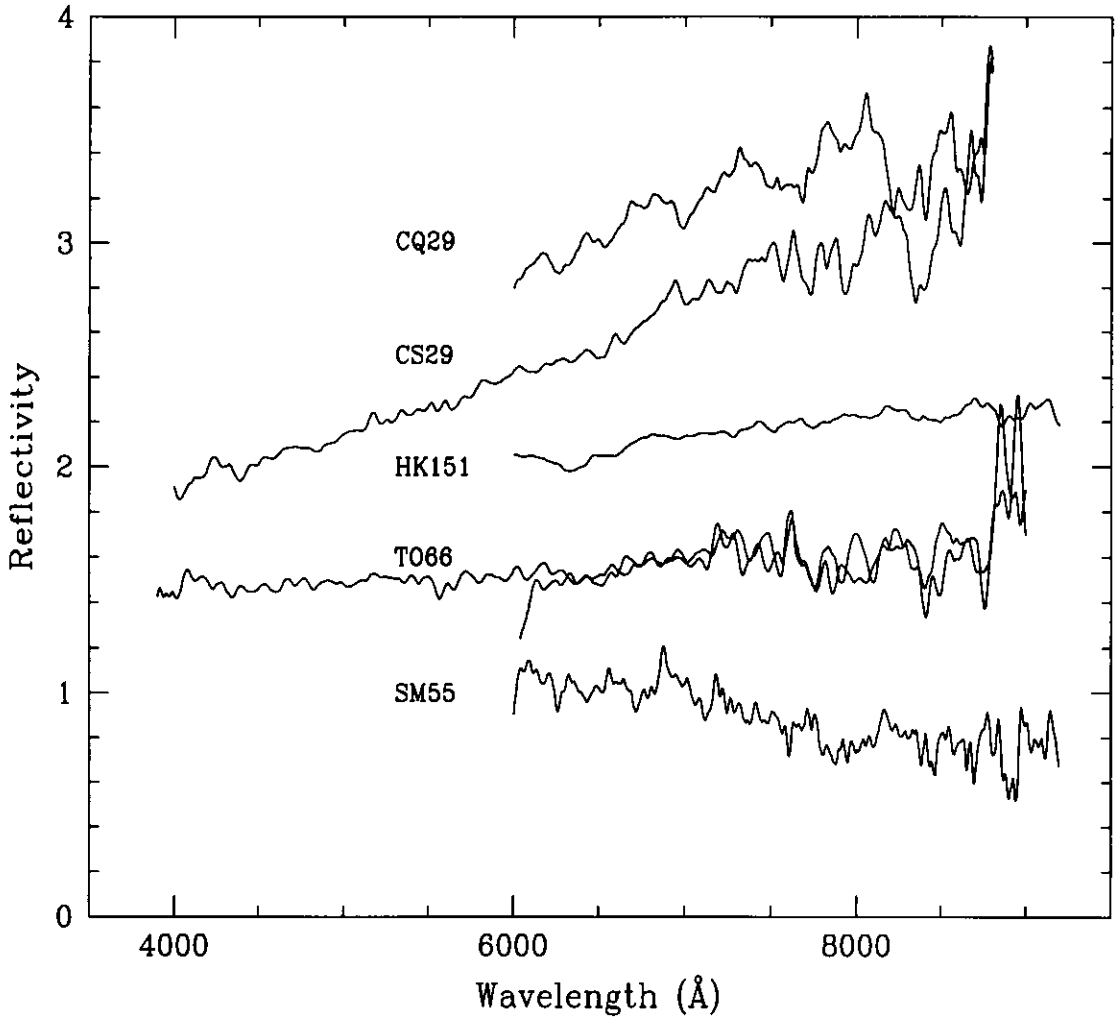

Figure 2.2: Reflectance Spectra of 1995SM55, 1996TO66, 1997CQ29 and 1998HK151. The scatter beyond 750nm is due to incomplete subtraction of strong skylines. The reflectance spectra of the individual objects are offset by an arbitrary value for better display. For 1996TO66 the "red+blue" and the "red only" spectra are shown: the good overlap of both spectra proves that first order contamination in the red is negligible.

Properties of individual objects

Here, we present short portraits of the individual TNOs/Centaur observed. Their characterization is based upon our results and data published in literature. The objects are listed according to temporal order of designation.

1992QB1: the M_R brightness of 7.00 mag corresponds to an equivalent radius of 110 km (albedo = 0.04), i.e. 1992QB1 may be of medium size. According to our BVRI colour measurements this TNO is a typical red object (gradient of about 30 %/100nm). While our VRI colours are in good agreement (though more accurate) with those of Luu&Jewitt 1996 the B magnitude differs by 0.35 mag (ours being redder). This deviating B brightness explains why 1992QB1 was previously considered an outliers in the V-R versus B-V diagram. According to our data 1992QB1 falls pretty much in the centre of the red group of objects in both colour-colour diagrams (see Figure 2.6). One can speculate whether a change of the physical properties of the TNO or problems with the earlier B filter measurements (our favoured interpretation) are responsible for the colour change in B-V. Neither a visible spectrum nor near-IR data of 1992QB1 are available so far.

1993RO: this TNO is fainter and most likely smaller than 1992QB1 (see Table 2.1.3). The VRI colours are red (V-I spectral slope of 25 %/100nm). The published VRI data (Luu&Jewitt 1996b) are in agreement with ours, while their B-V index is even steeper. Visible spectroscopy and JHK data of this object are still missing.

1994EV3: this medium bright TNO (see Table 2.1.3) is a puzzling object. It appears to be very red according to the B-V and R-I indices measured by Luu and Jewitt (1996b) and in our own data of 1999. Contrary to this, 1994EV3 has only slightly reddish (Luu&Jewitt 1996b) to slightly bluish (ours) V-R colours. Unfortunately, no further observations (visible and near-IR) of this exceptional TNO are reported.

1995HM5: we have JH magnitudes of this object only. Taking the M_J value of 7.30 mag, this object would be one of the smaller TNOs known so far (about 65 km equivalent radius for albedo 0.04). Our J filter radius is not too different from the one (about 80 km) obtained in the visible wavelength range (Tegler and Romanishin 1998). The published BVRI colours (Tegler and Romanishin 1998, Barucci et al. 2000) assign an almost neutral colour gradient to 1995HM55. Our J-H value of 1.18 mag is, however, very red, but also very uncertain. If confirmed, it would make 1995HM5 a rather peculiar object (neutral in the visible, very red in near-IR) among the TNOs. Only colours of the object are measured so far.

Table 2.5: List of TNO and Centaurs Colours.

Object	U-B (mag)	B-V (mag)	V-R (mag)	R-I (mag)	B-I (mag)	V-I (mag)	V-J (mag)	J-H (mag)	H-K$_s$ (mag)
Sun	0.2	0.67	0.36	0.33	1.36	0.69	1.08	0.29	0.06
1992QB1		1.00±0.20	0.60±0.10	0.56±0.09	2.16±0.19	1.16±0.11			
1993FW1		0.97±0.11	0.62±0.05	0.46±0.16	2.05	1.08			
1993RO		1.07±0.12	0.57±0.09	0.65±0.09	2.29	1.22			
1993SB							$\leq$1.37		
1993SC		1.04±0.17	0.62±0.08	0.66±0.22	2.32	1.28	2.57±0.08		
1994ES2		0.71±0.15	0.94±0.15	0.97±0.15	2.62	1.91			
1994EV3		1.50±0.19	0.54±0.05	0.80±0.20	2.84	1.34			
1994JR1		1.01±0.18	0.57±0.15	0.52±0.12	2.10	1.09			
1994JS			0.85±0.07						
1994JV			0.78±0.06	0.59±0.05		1.37			
1994TB		1.03±0.11	0.76±0.09	0.65±0.15	2.44	1.41	2.54±0.11		
1994VK8			0.62±0.11						
1995DA2			0.55±0.11	0.50±0.16		1.05			
1995DC2			0.77±0.16	0.58±0.16		1.35			
1995HM5		0.67±0.12	0.50±0.07	0.31±0.09	1.48	0.81			
1995QY9		0.71±0.03	0.47±0.01	0.40±0.06	1.58	0.87	2.01±0.13		
1995SM55		0.68±0.06	0.26±0.04	0.39±0.04	1.33±0.06	0.65±0.04			
1995WY2		0.99±0.15	0.68±0.15	0.43±0.15	2.10	1.11			
1996RQ20		0.89±0.14	0.68±0.09	0.58±0.09	2.15±0.14	1.26±0.11			
1996SZ4							$<$1.41		
1996TL66	0.97±0.19	0.69±0.08	0.31±0.17	0.40±0.14	1.40	0.71	1.27±0.11	0.35±0.14	0.04±0.11
1996TO66	1.01±0.12	0.67±0.08	0.37±0.05	0.39±0.03	1.43	0.76	0.86±0.14	-0.21±0.17	0.81±0.15
1996TP66		1.04±0.24	0.66±0.02	0.57±0.14	2.27	1.23	2.16±0.07	0.17±0.06	0.02±0.09
1996TQ66		1.16±0.10	0.70±0.07				2.41±0.08	1.00±0.27	0.03±0.09
1996TS66		0.98±0.05	0.60±0.17	0.67±0.17	2.25	1.27	1.87±0.11	0.65±0.07	0.09±0.09
1997CR29		0.79±0.10	0.47±0.068	0.68±0.12	1.94	1.15			
1997CS29		0.89±0.08	0.72±0.06	0.54±0.05	2.15±0.07	1.26±0.06	2.06±0.03	0.31±0.16	0.36±0.23
1997CQ29		0.93±0.14	0.71±0.19	0.61±0.14	2.25	1.32±0.20	1.84±0.37	0.66±0.38	
1997CT29		1.01±0.12	0.72±0.07						
1997CU29		1.06±0.21	0.70±0.09	0.55±0.09	2.31	1.25			
1997QJ4							1.23±0.31		
1998FS144		0.96±0.12	0.63±0.07	0.27±0.09	1.86	0.90			
1998HK151			0.45±0.06	0.41±0.05		0.86±0.06			
1998WH24		0.83±0.06	0.64±0.04	0.39±0.04	1.86±0.06	1.03±0.06			
1998VG44		0.93±0.05	0.61±0.04	0.77±0.04	2.31±0.08	1.38±0.08			
1998XY95		0.93±0.23	0.65±0.14	0.77±0.16	2.35±0.24	1.42±0.18			
1999TC36		0.96±0.04	0.70±0.04	0.58±0.04	2.24±0.04	1.28±0.04			
2060 Chiron		0.70±0.02	0.37±0.03	0.35±0.04	1.42	0.72	1.20±0.30	0.30±0.30	0.10±0.20
5145 Pholus		1.27±0.10	0.78±0.03	0.77±0.02	2.82	1.55	2.59±0.02	0.37±0.02	-0.03±0.02
7066 Nessus		1.09±0.04	0.79±0.04	0.71±0.10	2.59	1.50	2.29±0.04	0.28±0.10	0.00±0.10
8405 Asbolus		0.75±0.04	0.44±0.03	0.52±0.03	1.71	0.96	1.65±0.02	0.37±0.06	0.09±0.05
10199 Chariklo		0.77±0.05	0.47±0.02	0.54±0.02	1.78	1.01	1.74±0.02	0.41±0.02	0.07±0.03
1995DW2		0.54±0.10	0.43±0.07	0.49±0.10	1.46	0.92	1.31±0.10		
1998TF35		1.02±0.11	0.71±0.06	0.57±0.09	2.30±0.13	1.28±0.10			

The measurements from this work and from literature were combined as described in the text. The TNOs are listed in the upper, the Centaurs in the lower part of the table.

1995SM55: this large (i.e. bright) TNO has VRI and a red spectrum measured. Both observations indicate that 1995SM55 is a neutral to slightly bluish object. The spectrum (see Figure 2.2) displays a somewhat bluer gradient although with a trend to flatten off beyond 800nm. This object had no colours or spectra published so far.

1996RQ20: another medium-sized object (M_R = 6.99 mag, equivalent radius = 110 km for 0.04 albedo). From its BVRI colours (gradient of about 30 %/100nm) this object appears to be a reddish TNO similar to 1997CS29. The only V-R measurement available from literature (0.44 mag; Tegler and Romanishin 1998) would classify this TNO as neutral, which is in clear disagreement with our data. No spectrum nor near-IR photometry of 1996RQ20 are measured so far.

1996TO66: the M_R brightness of 4.53mag is almost exactly identical with the one found from earlier photometry (Hainaut et al. 2000). It corresponds to an equivalent radius (albedo = 0.04) of 345km which would make this objects one of the largest TNOs known so far. Our new data – colours and spectra – classifies 1996TO66 to be a neutral object. The two available spectra of 1999 confirm the quasi-simultaneous photometric colours. A close comparison with the 1997 spectrum (Hainaut et al. 2000) shows marginal differences between the 1997 red (beyond 750nm) and 1999 blue-to-red gradients. The photometric colours of Dec. 1999 agree well with the ones measured earlier (Jewitt&Luu 1998, Barucci et al. 1999b, Hainaut et al. 2000). This implies that the change in the amplitude of the rotation light curve of this object observed between 1997, 1998 and 1999 had no or very little impact on the object colours and spectrum; (for a new study of the light curve of this TNO see Sekiguchi et al. 2001). 1996TO66 is a representative of the neutral colour TNOs and it is considered the most interesting TNO observed so far: water absorption in H and K band (Brown et al. 1999), light curve changes (Hainaut et al. 2000).

1996TP66: this rather bright and most likely large TNO is also a very red object (gradient of about 35 %/100nm, i.e. redder than 1997CS29). Our BVRI colours are in good agreement with the ones of Tegler and Romanishin (1998), Jewitt and Luu (1998) and Barucci et al. (1999b). In the near-IR its spectral slope gets flat with H-K being of solar value (Noll et al. 2000).

1997CQ29: with 110km equivalent radius (M_R = 7.05 mag) this TNO may be a medium size body in the Edgeworth-Kuiper Belt. The variability in the V filter brightness (0.38 mag, see Tables 2.2) is due to the body's rotation and may indicate an non-spherical shape (axis ratio $>$ 1.45) and/or albedo variations (factor $\sim$ 2) on its

surface. Our visible data indicate that this object may be very similar to 1997CS29: a typical red TNO (constant gradient of about 30 %/100nm from about 500 to 900 nm). The V-J and J-H colours appear to be larger as compared to 1997CS29 which may be due to the large uncertainty in our photometry and/or due to rotational variability over the long near-IR integration times. Our VRI photometry agrees with that of Tegler and Romanishin (1998), the V-J colour differs – by about 0.1 mag – from that of Davies et al. (2000) – possibly because of the rotation light curve of the object.

1997CS29: this object appears to be a large TNO (M_R of about 4.85mag or 290 km equivalent radius) with a red spectrum and red colours in the optical wavelength range. The featureless visible spectrum (see Fig. 2.2) displays a constant gradient of 27 %/100nm from 400 to 900 nm with only marginal indications of a somewhat smaller slope beyond 800 nm. The VLT BVRI colours agree with the spectrum. However, they disagree with the B-V colour published by Tegler and Romanishin (1998) (ours: 0.89 mag, Tegler and Romanishin: 1.17 mag); our (quasi-simultaneous) spectrum and photometry does not support such a strong reddening in the blue wavelength range as indicated by the B-V value of Tegler&Romanishin. The Calar Alto results for BVRI lie in between the ones from the VLT and Tegler&Romanishin. They agree with the VLT ones for adjacent filter colours within the error bars, but they have a trend to a slightly redder gradient such that the B-I and V-I colours clearly deviate from the VLT ones. From our Calar Alto R band monitoring of this object over 3 nights (unpublished) we conclude that 1997CS29 is a slow rotator with a rotation period clearly longer than one day. Therefore, the discrepancy between the three data sets is either intrinsic to this object or due to inconsistencies in the data reduction of the various groups. In the near-IR filters JHK_s the colour reddening becomes smaller with a clear trend to level off toward the long wavelength end. 1997CS29 appears to be a typical representative of the red TNO population (B-I spectral gradient agrees with peak value in TNO population statistics; see section 2.1.4).

1998HK151: this medium-sized/bright object ($M_R = 6.87$ mag, equivalent radius of 120 km for albedo 0.04) belongs to the group of TNOs with neutral to only very slightly red colours. The spectral gradient of 7 %/100nm obtained from our VRI colours is in exact agreement with the one measured in our spectrum. This spectrum is the best one we have in terms of S/N (we had 0.4" seeing during the 1 hour integration time), but it is still not good enough to search with success for absorption bands in the red

part of the spectrum. However, a small turn-over to a flatter slope is found beyond about 800 nm. The object was measured with almost constant V filter brightness in two subsequent nights. No comparison data are available from literature.

1998TF35: the only Centaur in our sample is of about 50km size (according to its absolute brightness in R). It is a red object more like the typical red TNOs, but not as red as the two other red Centaurs, 5145 Nessus and 7066 Pholus (Barucci et al. 1999b and references therein). No comparison data of this object are found in literature.

1998VG44, 1998XY95, 1999TC36: these TNOs, although different in their absolute magnitude and thus possibly in size, have very similar BVRI colours. They all belong to the group of typical red TNOs with colour gradients of 30-40 %/100nm. Our measurements for 1998VG44 are in agreement with the ones of Romon et al. (2001) except for R-I for which the deviation is slightly higher (0.05mag) than compatible with the claimed photometric errors. Near-IR data of all three objects are not available.

1998WH24 one of the largest TNOs measured so far (M_R=4.68mag, equivalent radius of about 350km for albedo 0.04) shows intermediate red colours. The I band brightness would indicate an unusual R-I gradient, but it is most likely contaminated since the photometry was done in the immediate neighborhood of a bright star (the given uncertainty is a formal error). This is also apparent when comparing our data with those of Barucci et al. (2000): while B-V and V-R agree within the error bars, R-I does not. No spectra and near-IR data of this TNO are published so far.

In summary: in our ESO and Calar Alto observations from 1998 to 2000 we could identify

- 4 neutral, slightly bluish or slightly reddish TNOs (1995SM55, 1996TL66, 1996TO66, 1998HK151),
- 1 intermediate red TNO (1998WH24),
- 9 red TNOs (1992QB1, 1993RO, 1996RQ20, 1996TP66, 1997CQ29, 1997CS29, 1998VG44, 1998XY95, 1999TC36),
- 1 red Centaur (1998TF35)
- 2 TNOs appear as outliers (1994EV3, 1995HM5).

Table 2.6: Merged List of TNO and Centaurs Spectral Gradients.

Object	Grad(B-I) (%/100nm)	Grad(V-I) (%/100nm)	Grad(V-J) (%/100nm)
1992QB1	30	21	
1993FW1	25	17	
1993RO	38	25	
1993SB			<4
1993SC	39	29	44
1994ES2	61	82	
1994EV3	81	33	
1994JR1	27	18	
1994JV		35	
1994TB	47	37	42
1995DA2		16	
1995DC2		33	
1995HM5	3	5	
1995QY9	6	7	20
1995SM55	-1	-1	
1995WY2	19	3	
1996RQ20	30	27	
1996SZ4			<5
1996TL66	1	1	3
1996TO66	2	3	-3
1996TP66	36	26	25
1996TQ66			36
1996TS66	35	28	16
1997CR29	20	21	
1997CS29	30	27	22
1997CQ29	35	31	15
1997CU29	39	27	
1997QJ4			2
1998FS144	16	8	
1998HK151		7	
1998WH24	16±2	15±3	
1998VG44	39±5	35±5	
1998XY95	41±16	38±13	
1999TC36	35±2	29±3	
2060 Chiron	2	1	2
5145 Pholus	79	48	45
7066 Nessus	58	44	30
8405 Asbolus	11	11	10
10199 Chariklo	13	14	2
1995DW2	3	9	3
1998TF35	38±8	29±6	

The TNOs are listed in the upper, the Centaurs in the lower part of the table.

With a few exceptions, our colour values confirm the ones reported for the respective objects in literature. In the few cases for which spectra of TNOs are available, the spectroscopic colour gradients are in good agreement with the ones determined from (quasi-simultaneous) photometric data.

2.1.4 Photometric Characterization of TNOs and Centaurs

For the group characterization of TNOs and Centaurs we apply colour-magnitude and colour-colour diagrams as well as the statistics of colour gradients, for the two latter we compare the two object groups TNOs and Centaurs.

The colour-magnitude diagram uses only our own measurements of TNOs, while the colour-colour plots and the colour gradient statistics are based on a compilation for TNOs and Centaurs which merges the results of our measurements with the table of object colours as published by Barucci et al. (1999b), supplemented by those of Barucci et al. (2000) and Romon et al. (2001). The following modifications of the original table of Barucci et al. (1999b) were applied: (a) data of objects measured for the first time(1995SM55, 1998HK151, 1998TF35, 1998VG44, 1998XY95, 1999TC36) are included, (b) for object colours, for which we consider – based upon the discussion in section 2.1.3 – our own results more reliable than those in literature, our values replace those from other sources (1992QB1, 1996RQ20, 1997CS29, 1997CQ29, 1998WH24), (c) object colours are added if measured for the first time (1993EV3, 1995HM5).

Table 2.5 lists the merged new table of broadband colours for TNOs and Centaurs. It considers our own measurements of 17 objects and the published data of 39 objects. The merged table contains 37 TNOs and 7 Centaurs. The low number of Centaurs with photometry measured, makes statistical conclusions on group properties very difficult. At best first trends can be derived. For TNOs the near-IR range is not yet covered by a large enough set of measured objects such that for the time being we will not include it in our statistical analysis.

Colour-magnitude diagram

Fig. 2.5 shows the V-I colour versus the absolute magnitude M_R of the objects in the R band filter (see Table 2.1.3). Over the whole range of absolute magnitudes measured our data show no conclusive correlation between M_R and the V-I colours of the objects. At best – however based on only 6 data points – one could hypothesize a linear trend between M_R and V-I for the brightest TNOs (brighter than $M_R = 5$ mag). The absence of a clear relationship between M_R and V-I in Figure 2.5 is in contrast with the results published by Jewitt&Luu (1998) and Davies et al. (2000) (see Fig. 2.3).

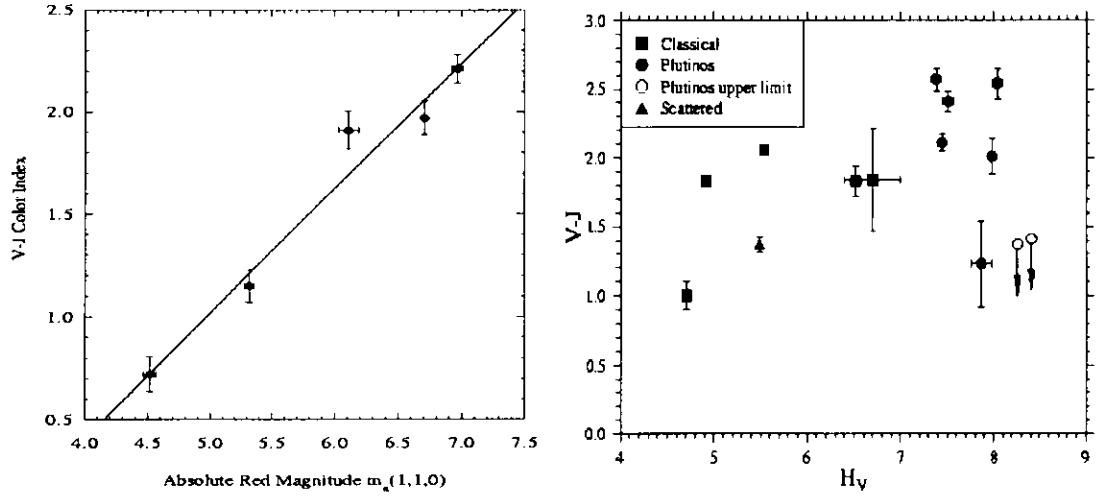

(a) Luu & Jewitt (1998) reported an apparent correlation

(b) Davies *et al.* (2000) reported the correlation with selected objects

Figure 2.3: Previous results of colour-Magnitude Diagram. Plot of red absolute R magnitude versus the $V - J$ colour index

Both groups found a strong correlation between M_V and V-J using a sample of only 5 selected TNOs with high-quality measurements. The line in Fig. 2.3 (a) shows a least-square fit to their TNOs data for V-I. The linear correlation coefficient is $r_{\rm corr} = 0.98(N = 5)$. Davies et al., however, cannot confirm this correlation using a larger sample of 14 TNOs.

Here, we present new measurements and the plot of colour (V-I) – absolute magnitude diagram. For the purpose of comparison to our data, V-I data of Jewitt&Luu (1998) ware plotted in Fig. 2.4 and $r_{\rm corr} = 0.95$ ($N = 5$) in this case. However, our sample also suggests that the colour dispersion does not depend on M_R, i.e. on the product between

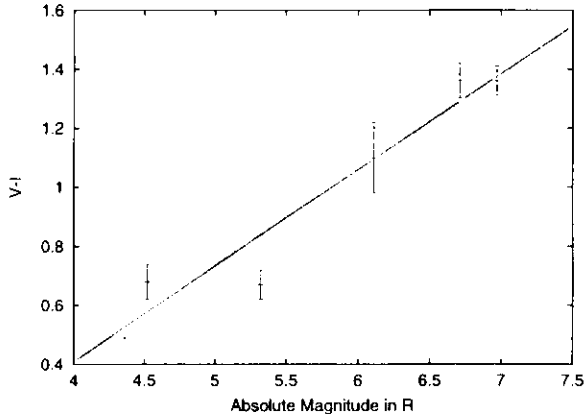

Figure 2.4: Colour – Absolute magnitude diagram of TNOs and Centaurs. For the purpose of comparison to our data, V-I data ware plotted from Jewitt&Luu (1998).

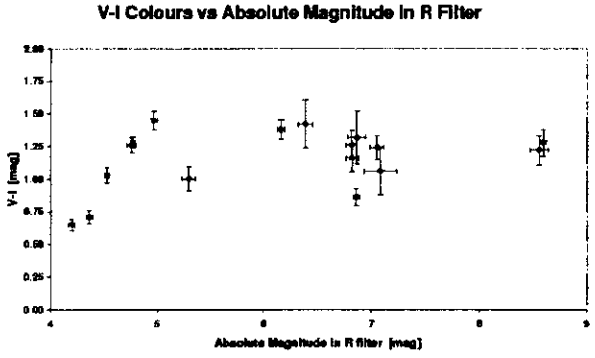

Figure 2.5: Colour – Absolute magnitude diagram of TNOs and Centaurs. The figure plots the V-I colour of our own TNO&Centaur measurements versus the absolute magnitude as derived from the R filter brightness of the objects. The plot includes 16 TNO and 1 Centaur measurements.

cross-section (or size) and albedo of the object. The linear correlation coefficient for our data is $r_{corr} = 0.25(N = 15)$. This statistical number imply that the correlation between size and colour is little. A larger statistical sample needs to be analyzed to confirm or disprove this suggestion.

Colour-colour diagrams

Three colour-colour plots are presented using the merged data set of Table 2.5: B-V versus V-R, B-V versus R-I, and V-R versus R-I (Fig. 2.6). While – on a first sight – the B-V vs V-R diagram suggests a certain population clustering among the TNOs (a neutral and a red population), only a single group of TNOs with continuous increase in reddening is seen in the two other colour-colour plots.

TNOs: the B-V vs V-R plot gives the impression that there are two groups of TNOs: one with neutral to slightly reddish colours, one with red to very red colours. This interpretation is already described by Tegler&Romanishin (1998) who argue for the existence of two distinct TNO populations (see Figure 2.1). The separation of the two groups is in B-V (and not in V-R) with objects missing for B-V = 0.7 (i.e. almost solar colour) to 0.9 mag. Considering the large error bars and the presence of a few objects in or close to the B-V gap, an overlap of both groups cannot be excluded. New observations of a TNO sample of about 15 objects (Trujillo et al. 2000) do not show population clustering. A two-dimensional Kolmogorov-Smirnow statistics analysis of the available colour data (Hainaut, priv. communication) concludes that the observed colour distribution (this includes also B-V vs V-R) is compatible with both a single continuous as well as with a double peak colour population of TNOs.

It is noteworthy that the TNOs of solar-type B-V population have also neutral V- R and R-I colours. The red B-V group objects are also red in V-R and R-I. This confirms the conclusion from our spectroscopy measurements that usually no sudden and significant changes of the spectral slope are seen in optical spectra of TNOs (see also section 2.1.3).

Two outlier objects are found in both colour-colour plots: 1994ES2 and 1994EV3 (the two other objects away from the main group are 1992QB1 and 1996TL66, but we believe that this is due to wrong measurements published in literature – see section 2.1.3).

Centaurs: the measured Centaurs – although small in number – seem to be either mostly neutral to slightly red or very red objects (5145 Pholus and 7066 Nessus). Three out of the 4 Centaurs with neutral colours fall in the B-V range of 0.7-0.8 mag, i.e. they appear in the B-V gap of the TNO population. 3 red Centaurs are placed at the upper end and beyond the red TNO group in the B-V vs V-R diagram (Fig. 2.6).

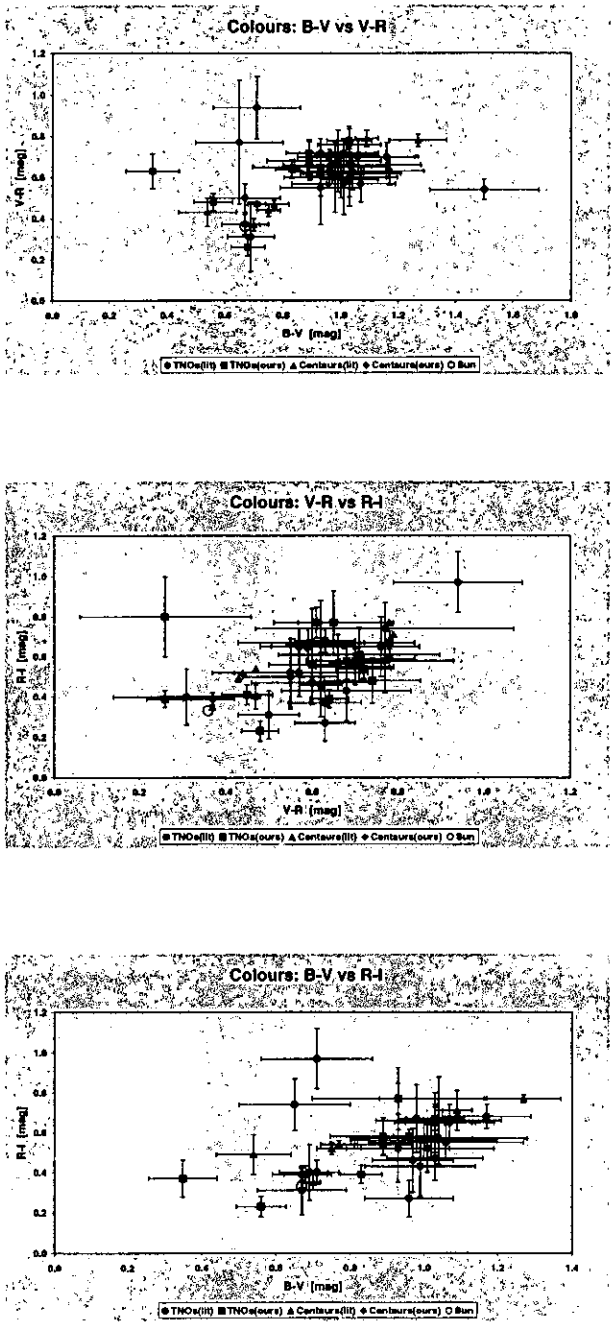

Figure 2.6: Colour-colour diagrams of TNOs and Centaurs. Top: B-V versus V-R; Middle: V-R versus R-I; Bottom: B-V versus R-I. The plots compare our own measurements with data from literature. Solar colours are indicated by a circle.

Colour gradient statistics

Table 2.6 lists the colour gradients (or reddening) of the TNO and Centaurs as calculated from the colours of Table 2.5. For the colour gradient statistics the number of objects per gradient interval is counted. The gradient intervals are set in steps of 10 %/100nm over the total gradient interval measured (which was -10 to 100 %/100nm). The chosen step width is approximately twice the average standard deviation of the majority of the individual gradient values. Although of arbitrary nature, this selection grid may somehow represent groups of objects with distinct differences in surface reddening. The gradient statistics obtained are presented in Figs. 2.7. The reddening of the objects (in %/100nm) as compared to the Sun is calculated according to Equation (2.1) and the number of objects (Y axis) per reddening interval (X axis) is counted. The sub-panels show the results for three different colour gradients, in each diagram separately for TNOs and Centaurs.

For TNOs the gradient statistics suggests the following conclusions:

- the majority of TNOs has reddening between 0 and 50 %/100nm for all three colour gradients considered; only a few objects have higher reddening in B-I and V-I, none in V-J.
- the distribution maximum falls between 20 – 40 %/100nm for the B-V and V-I gradients with a trend to smaller gradient values for V-I. The V-J plot gives an inconclusive result because of its low number statistics, although a general trend to smaller reddening gradients (as compared to B-I and V-I) seems to be present.
- the B-I and V-I gradient distributions of TNOs may be double-peaked: the group with gradients of 0 – 10 %/100nm may be small, the other one with 20 – 40 %/100nm reddening is more abundant in number. However, the statistical significance of the group with neutral colours seem to be low (since the number of objects with colour gradients of 10 – 20 %/100nm is almost as high as the neutral ones).

The trend of smaller reddening gradients toward longer wavelength in the visible region is in qualitative agreement with results from the near-IR photometry which gives close to zero reddening for several TNOs in H-K (see Davies et al. 2000; Noll et al. 2000). From our spectra, we have – marginal – indications that this change toward smaller reddening gradients gradually starts between 700-800nm.

For Centaurs we conclude from the colour gradient plots:

- the Centaurs show up in two separate reddening ranges: the majority (in total 4) falls in the reddening interval between 0 – 20 %/100nm, a minority has gradients of more than 30 %/100nm. This applies for all three colour gradients considered.

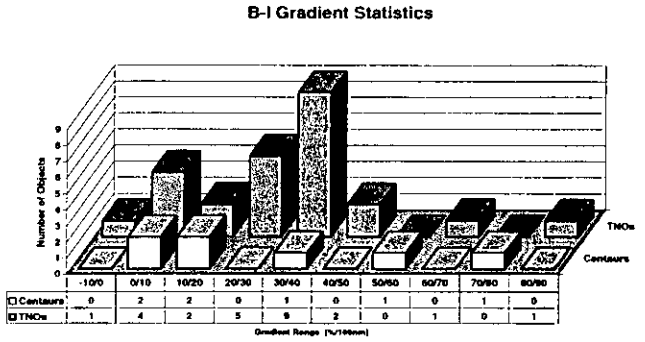

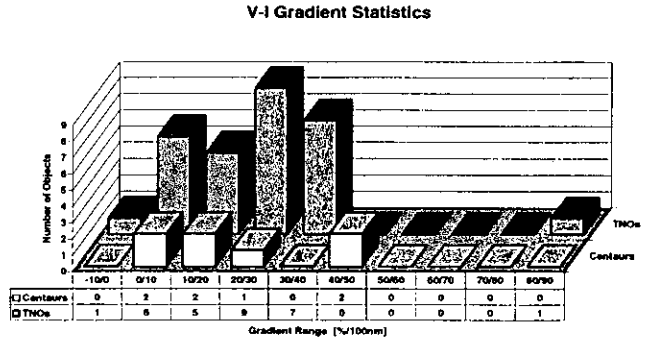

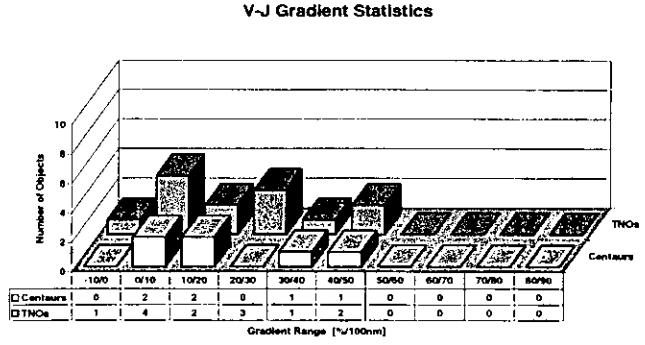

Figure 2.7: Reddening gradient statistics of TNOs and Centaurs. Top: B-I gradient statistics, Middle: V-I gradient statistics, Bottom: V-J gradient statistics. The explanations of each axis and data are in the text.

- the Centaurs of neutral colour tend to be "clustered", while the red objects spread over a wide gradient range.
- the number statistics of measured objects is very poor (only 7 in total). Therefore, the two conclusions mentioned above have to be taken with great care.

The gradient statistics suggests a diversity in the pre-dominant reddening between TNOs and Centaurs: the majority of TNOs has typical reddening of 20 - 40 %/100nm, while only one Centaur in this colour gradient range was found (so far). The measured Centaurs seem to populate either the blue to slightly reddish or the extremely red colour gradient ranges. Therefore, if Centaurs are considered to be sunward scattered TNOs (Levison 2001), these objects have likely undergone a colour change as compared to the TNOs in the Edgeworth- Kuiper-Belt.

The colour palette seen in objects of the outer solar system is usually attributed to the combined action of three effects:

(1) High-energy radiation which could turn the ice-carbon mixture on the surface into complex hydrocarbon compounds of reddish colour. According to Shul'man (1972) the time scale for in-situ growth of an irradiated mantle (of several 10cm thickness) is of the order of 10^7 to 10^9 years. Thin mantles grow faster which may imply that colour changes due to irradiation reddening may happen on time scales of a few million years.

(2) Fresh ices from below the surface can be excavated by impacts of other objects. The ices from the crater area can be distributed over a wide surface range. Assuming that a major part of the surface is covered by fresh cratering deposits, the neutral surface colours may be explained. As demonstrated by Luu&Jewitt (1996b2), impact resurfacing – in combination with the high-energy radiation reddening – can produce any colour value observed in TNOs and Centaurs, depending on the collision rate or in other words the size distribution of the objects. The latter also defines the typical time scales for the impacts with significant resurfacing potential. Luu&Jewitt confirm the typical collision time scales of 10^6 to 10^7 years for the Edgeworth-Kuiper-Belt region, first published by Stern (1995).

(3) Intrinsic activity like in comets could produce a coma of volatile gases (N_2, CO like in the atmosphere of Pluto) around TNOs and Centaurs which can re-condense (at least in parts) back onto the surface, thus forming a fresh ice layer. This scenario is proposed by Hainaut et al. (2000) to explain the light curve change observed

in 1996TO66. Although the surface temperature of the TNOs is very low (40-50K) and only N_2 as well as CO and CH_4 ices may be able to sublimate on a very low level, atmospheric frost would have the same effect as impact resurfacing, i.e. producing neutral colours of the objects' surfaces. At present, no estimations of time scales for resurfacing by intrinsic activity are available. Obviously, the process of ice recondensing on the surface must be fast, if it shall explain the 1996TO66 case.

Interpretation of the spectral diversities in TNOs and Centaurs: Centaurs orbit the Sun at distances where collisions with other Solar System bodies are less likely (since the space between the major planets doesn't seem to be very populated with minor bodies). On the other side, since they get closer to the Sun, internal activity may be triggered more frequently and stronger due to more efficient solar heating of the surface layers. Therefore, cometary activity like that observed in the Centaur 2060 Chiron may cause resurfacing of Centaurs with freshly condensed frost and may account for the neutral to slightly reddish object observed. If the intrinsic activity is not triggered (for instance due to strong crust formation on the surface), very red colours could develop with time due to high-energy radiation. Hence, a bimodal colour gradient distribution with very bluish and very red objects only – as seen in Figs. 2.6 and Figs. 2.7 – may result among the Centaurs. Although one could speculate that the closer the perihelion to the Sun, the more neutral coloured Centaurs should be found (because of enhanced coma activity), this correlation may be overruled by the individuality of the objects: Pholus, having a similar perihelion distance as Chiron and a similar aphelion distance as 1995DW2, is the reddest Centaur known so far, while Chiron and 1995DW2 appear to be of neutral or only slightly reddish colour. This may indicate that a thick reddish crust of hydrocarbons may have formed on the surface of Pholus by high-energy radiation and neither impacts nor cometary activity happened over the last couple of million years, the typical dynamical life time of objects in Centaur orbits (Levison 2001).

Since TNOs orbit the Sun at larger distances (i.e. they should experience less internal activity), in the more populated Edgeworth-Kuiper-Belt region (i.e. they are exposed to more collisions), their surface colours may be the result of a rather complex balance of impact and activity resurfacing on one and radiation reddening on the other side. Assuming for instance a much longer resurfacing time scale than for Centaurs, the colour gradient distribution of TNOs would show – on the average – more redder objects than the Centaurs' one. This can explain the "red-shifted" peak in the gradient statistics of TNOs as compared to the Centaurs.

In other words: a "red-shifted" TNO populations as compared to the Centaurs (ignoring extreme cases like Pholus and Nessus) suggests that activity resurfacing plays a

much larger role for the Centaurs than for the TNOs. Since Centaurs are believed to be sunward migrating TNOs, this scenario also implies that TNOs change colours when becoming Centaurs (trend to neutral colours).

Generic differences in the constitution and chemistry of TNOs has been suggested (Tegler&Romanishin 1998) as explanation for the double peak distribution of TNOs in the B-V vs V-R (see Fig. 2.6 and less pronounced in the B-I gradient plot of Fig. 2.7). An alternative hypothesis could evolve from the assumption of two populations of TNOs: one which is subject to radiation and collision resurfacing only and one which in addition experiences also resurfacing by cometary activity. The latter hypothesis has the advantage of explaining the observed distribution without needing an additional ad-hoc population of different physical nature.

Both scenarios, i.e. the one for the development path of TNOs toward Centaurs and the alternative explanation for the double peaked colour distribution of TNOs are built on very weak trends in the gradient or colour distributions of TNOs and Centaurs. Due to the low number statistics in both cases they are to be considered as uncertain and very speculative for the time being. In particular, more Centaurs need to be measured to put the colour statistics of these objects on safer grounds.

2.1.5 Conclusions

Over the past 2 years we have collected photometric data of 16 TNOs and 1 Centaur plus spectra of 5 TNOs. The photometry contributed mostly to the existing data set in the visible wavelength range.

- Consecutive colour diversity from solar colour to reddened colour was found rather than 2 distinct population proposed by Tegler and Romanishin (1998).
- Absolute magnitudes measured our data show no conclusive correlation between M_R and the $V - I$ colours of the objects on the contrary to Luu and Jewitt (1998).
- The spectroscopy delivered featureless spectra with spectral gradients which confirm - in principle - the correctness of spectral gradient estimates from broadband filter photometry.
- No absorption band due to surface material was found from the optical spectra.

On the contrary of former classification study, our results show the continuous diversity from solar to reddened colour of their surface. All icy bodies have suffered from their surface reddening by the high energy particle and the solar UV irradiation over the age of the solar system (Khare *et al.*, 1984). The carbonized compounds of the surface volatiles which was transmuted into more complex, polymerized material by irradiation, attribute to reddening. TNOs and Centaurs should suffer from resurfacing process as well.

Since TNOs suffer from collisional erosion with dust and small debris, the impact resurfacing may play an important roll on the resurfacing process. On the other hand, active objects like Chiron and possibly TNO 1996 TO_{66} can produce their new surface while they are active. The fall-back debris by cometary activity coat their surface. Chiron's neutral colour can be explain by this assumption. However, a comprehensive quantitative model has not been established, owing to the lack of the knowledge about cometary activity of icy minor bodies.

The possibility of cometary activity for the icy minor bodies in addition to Chiron, the measurements of the sublimation rate of volatile ices, and the knowledge of chemical composition of volatile ices are needed to explain the resurfacing process.

2.2 Bi-colour Lightcurve of TNO 1996 TO_{66} search for cometary activity and surface albedo variation

In this section, lightcurve observations to obtain the evidence of intrinsic activity of a TNO are described. A change in the shape and amplitude of the TNO 1996 TO_{66}'s light-curve between Sep.1997 and Sept.1998 was reported by Hainaut et al. (2000).
Time-resolved bi-colour photometry, together with high spatial resolution imagings using the ESO VLT 8.2m were performed in optical in order to verify and monitor the lightcurve change, to address potential colour variation with rotation phase and to search for the presence of a cometary coma. These observations can be the starting points for a challenging work of surface mapping of TNOs.

1996 TO_{66} is one of the brightest TNOs discovered so far. The orbit is classified as cubewano-type, i.e. not in resonance with Neptune. Its rotation period was measured to be 6.250 $\pm$0.029h (Hainaut *et al.* 2000). Visible spectra and broadband filter observations in the visible and near-IR show neutral surface colours similar to Chiron (Boehnhardt *et al.* 2001). Brown *et al.* (1999) reported absorptions near 1.5 and 2.0 μm in the near-IR spectra and attributed them to surface water ice. It was the first such detection on a TNO. They also reported that the intensity of the water bands in the spectrum varies with rotation phase, suggesting a "patchy" surface like Pluto (Young *et al.* 1999). This is further supported by the asymmetric lightcurve observed almost simultaneously by Hainaut *et al.* (2000) which is difficult to explain without albedo variation. As mentioned above, the authors suggested a short-lived cometary outburst in 1996 TO_{66} as the origin of rather peculiar long-term changes seen in the rotation lightcurve of this TNO: (1) during the 1997 runs, the object displayed a nearly symmetrical double-peak lightcurve with a full amplitude of 0.12 mag in R; (2) in 1998 the 6.25 h lightcurve had only a single maximum with a full amplitude of 0.38 mag in R. Various possible explanations for this change were considered and a short-lived cometary outburst was favoured.

In order to study the surface variations of TNOs, we carried out time resolved, high spatial resolution imaging of 1996 TO_{66} to verify the lightcurve change, to address potential colour variation with rotation phase and to search for the presence of a cometary coma.

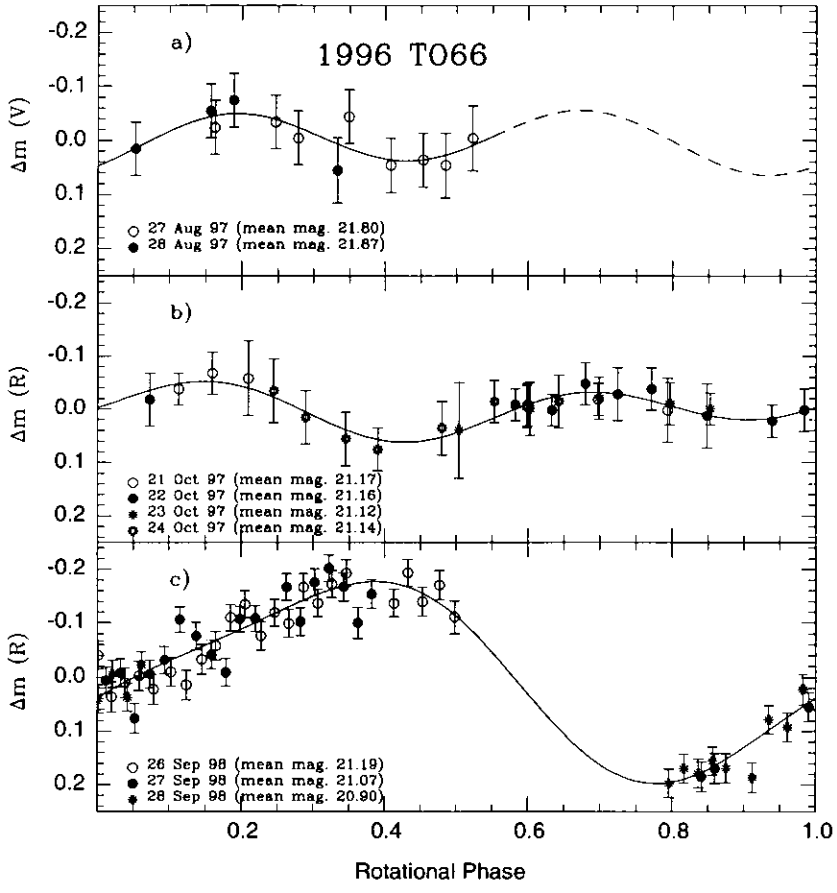

Figure 2.8: A change in the shape and amplitude of the Trans-Neptunian Object 1996 TO_{66}'s light-curve between Sep.1997 (double-peaked lightcurve, amplitude = 0.12 mag) and Sept.1998 (single-peaked lightcurve, amplitude = 0.3 mag) was reported by Hainaut *et al.* (2000).

Table 2.7: Characteristics of Orbital Elements of 1996 TO_{66}

semimajor axis	43.49 (AU)
eccentricity	0.114
inclination	27.38 (degree)
orbital period	241.8 (year)
Orbit type	cubewano

Notes: Orbital Elements were published on MPEC 2000-P19.

2.2.1 Observations at ESO VLT

1996 TO_{66} was observed with the ESO-VLT Antu telescope (UT1) and the FORS1 instrument on Paranal Observatory, Chile. FORS is a FOcal Reducer and low dispersion Spectrograph, which supports 2 image scales depending on the collimator used. The high resolution mode used for our images has a pixel scale of 0."1 on the 2048 $\times$ 2048 24 μm CCD pixel. The images were obtained in Service Observing mode by the Paranal Observatory staff: the first run was done on Nov. 14, 1999, the second one on Dec. 12, 1999. Both runs were phased in order to obtain a complete coverage of the 6.25 h rotation period of this TNO. The exposure series consisted of a sequence of alternating jittered R and V images continuously executed over several hours in order to sample the lightcurve and the colour variations, which can reflect albedo changes of the surface. In this way the goal of time-resolved photometry could easily be combined with the second one, i.e. to get deep and high spatial resolution images. In order to get sufficient S/N ratio, the individual

Table 2.8: Characteristics of the Filters

Filter	λ_0	FWHM
Bessel R+36	657 (nm)	150.0 (nm)
Bessel V+35	554 (nm)	111.5 (nm)

exposure time was set to 300 sec. in Bessel V and R filters. Although sidereal tracking was applied, the trailing of 1996 TO_{66} due to its motion was 0."14, 0."02 in Nov. and Dec., respectively. Those values are much smaller than the average seeing size measured from field stars in the images (0."55 and 1."05 in R, 0."61 and 1."15 in V, respectively).

The photometric parameters of the equipment and the atmosphere were determined by observing various standard star fields (PG2331, Rubin 152 from Landolt, 1992) at

different airmasses. Beside that, the usual calibration frames (biases, darks, sky flatfields) were taken. Table. 2.9 summarizes the observing geometry and conditions.

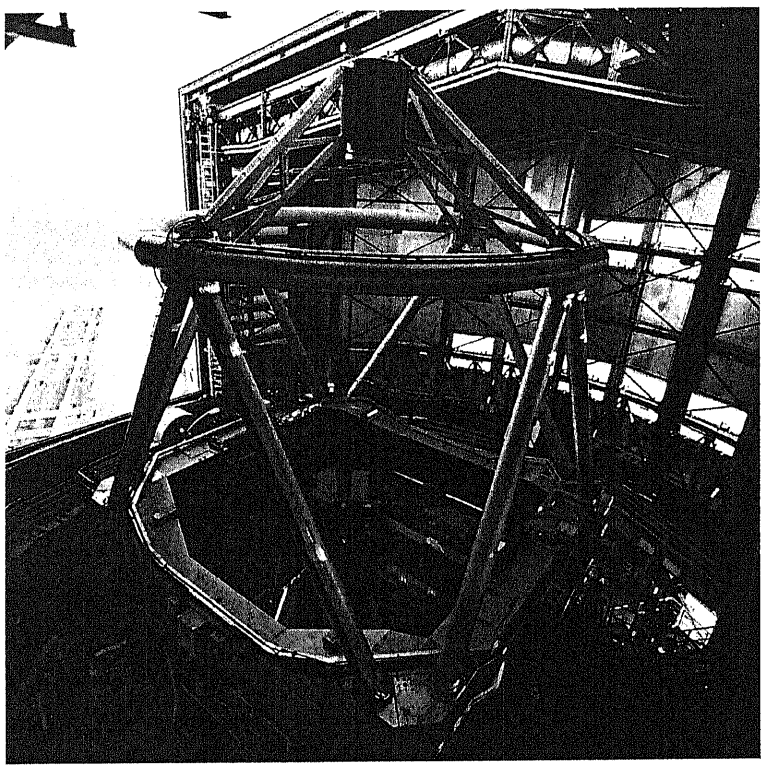

Figure 2.9: The ESO Very Large Telescope (VLT) at the Paranal Observatory (Atacama, Chile) is one of the world's largest and most advanced optical telescope. It comprises four 8.2-m reflecting Unit Telescope.

During the photometric nights, various standard stars were observed at different airmass by the ESO Paranal staff to derive the extinction coefficients and colour coefficients. We could get the photometric zero points of these system with Landolt standard fields, PG2331, Rubin 152 (Landolt, 1992).

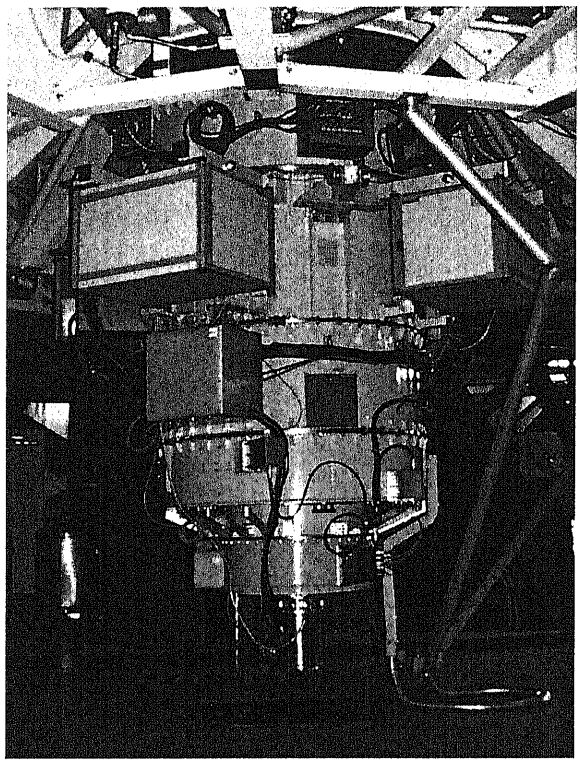

Figure 2.10: CCD array of FORS (FOcal Reducer and low dispersion Spectrograph). This instrument supports 2 image scales depending on the collimator used. The high resolution mode has a pixel scale of 0."1 on the 24 μm of 2048 $\times$ 2048 pixels CCD array.

Table 2.9: Observing Circumstances for 1996 TO_{66}

Epoch	R.A.(2000)	Dec.(2000)	$\dot{\alpha}\cos(\delta)$	$\dot{\delta}$	R_h	Δ	Phase Angle	Elevation
UT	hh mm ss	hh mm ss	"/h	"/h	AU	AU	degree	degree
14 Nov. 1999	23 57 12	+03 22 16	-1.58	-0.60	45.96	45.33	0.95°	62.0 - 36.2°
12 Dec. 1999	23 56 32	+03 18 26	-0.23	-0.06	45.97	45.77	1.20°	59.9 - 22.1°

The equatorial coordinates (J2000.0) and motions are listed for the mean epoch of the observations. R_h, Δ, $\dot{\alpha}\cos(\delta)$, $\dot{\delta}$ are the heliocentric distance, the geocentric distance, the velocity in the Right ascension and the velocity in the Declination, respectively

2.2.2 Image Processing

Bias and Flatfield

A template bias frame was created as follows: two sets of 5 bias level exposures were medianed. The resulting frames were again averaged to get the template. This template bias was then subtracted from all object, standard star and sky flatfield frames. "Super-flatfields" could be created for each filter for the November data using 2 D wavelet transformation technique. The high and middle frequency components of twilight sky flatfields and low frequency components of night sky flatfields were combined. The night sky flatfields were computed as median of jittered object frames. This method is described in detail in Hainaut *et al.* (1998). For the December data, the jittering of the images was not sufficient to make a high-quality median flatfield. Therefore, we adopted normal twilight sky flatfields. This may be one of the reason for the larger scatter measured in the December data (*see* below). After flatfielding, the cosmic rays were carefully removed from the images. At the end, in order to avoid effect from the moonlight and gradients from the sky emission in the images, we corrected each image for the sky background level using 2 D fit of the background pixel levels by 3rd degree polynomial function. 1st order flux calibration of the images was obtained using the standard star fields observed during the night and system calibration parameters for the instrumentation used (*see* ESO web page).

Composite image

In order to investigate the possibility of a coma around 1996 TO_{66}, all frames obtained in both filters during each run were re-centered on the object and stacked. Figure. 2.11 displays the composite of 18 R filter images of in total 5400s integration time of 1996 TO_{66} in November, 1999. The FWHM of the TNO and star images in this composite is 0.59 sec.

Differential photometry

Differential photometry is applied to improve the absolute photometry for the lightcurve analysis. We could select 18 comparison stars for the November data, 12 comparison stars for the December data following the rules to choose (1) as many stars as possible, (2) stars as bright as possible, (3) with maximum exposure level below 55000 ADU to keep the linearity of CCD detector. (4) stars that are present in the whole set of images. This

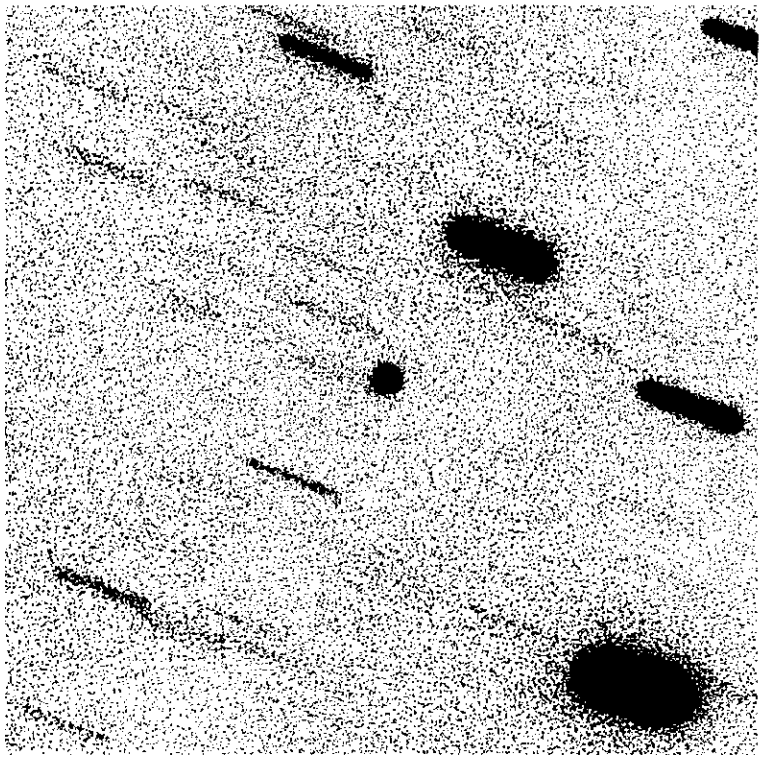

Figure 2.11: The sum of 18 individual images of 1996 TO_{66} in November, 1999, with an effective integration time of 5400s. 1996 TO_{66} in in the center and the star appear in segment bars because the images have been shifted to cancel out the motion of 1996 TO_{66}. The dimensions of the image are 51" $\times$ 51"; North is to the top, and East is toward the right.

ensured an excellent correction of all potential extinction variations and for second order extinction variations.

2.2.3 Results

Radius

We measured 18 images for November and 11 images for December data by aperture photometry method. For non-active solar system spherical bodies, their apparent magnitude due to scattered sunlight is given by the following relation (Russell 1916),

$$p_\lambda \, \phi(\alpha) \, {r_N}^2 = 2.238 \times 10^{22} \, {R_h}^2 \, \Delta^2 \; 10^{0.4(m_{\odot\lambda} - m_\lambda)} \tag{2.2}$$

where R_h and Δ (AU) are the heliocentric and geocentric distances respectively, $m_{\odot\lambda}$ and m_λ are the apparent magnitudes of the Sun and the object (in our case of 1996 TO_{66}) at wavelength range λ, respectively, $\phi(\alpha)$ is phase factor to correct for phase angle α dependence, and p_λ is the geometric albedo at the corresponding wavelength.

At present, the phase function of TNOs and Centaurs is totally unknown. Therefore we used a linear approximation, $\phi(\alpha) = 10^{0.4\beta\alpha}$ with an empirical phase coefficient value β=0.04 mag/deg (as is typical for cometary nuclei, e.g. 2P/Encke – *see* Luu & Jewitt 1990 – 10P/Tempel 2 - *see* Jewitt & Luu 1989).

The geometric albedo of TNOs and Centaurs is also poorly known. Campins *et al.* (1994) derived an albedo: p=0.14 from the mid-IR observation of the Centaur Chiron. Altenhoff & Stumpff (1995) supported an albedo p=0.13 for Chiron from millimetre wavelength data at 250 GHz. However, these measurements were made when Chiron clearly exhibited a coma which contaminated the nucleus due to additional dust scattering. Therefore, these values should be regarded as an upper limit. Jewitt & Kalas (1998) derived p=0.045 for the Centaur Chariklo (1997 CU_{26}) in mid-IR, 20 μm. Recently, Thomas *et al.* (2000) reported the albedos of 2 TNOs, 1993 SC, 1996 TL_{66} as 0.022 and 0.030, respectively using *ISO* observations. However, the detection level was marginal. We adopt a 0.04 albedo as typical for cometary surface albedo of 0.04 (1P/Halley), which allows us the direct comparison of our radius estimates to previous results obtained with this value by other groups. The various results for 1996 TO_{66} are listed in Table. 2.10. The error of photometry for our composite data comprises the complete error budget, i.e. skynoise, measurement statistics and photometric calibrations.

The derived radius of 1996 TO_{66} is about 340 km in R, 310 km in V. One of the reason for this difference between R and V is that we used same albedo value for each. On the other side, non-averaged measurements over the rotation phases can cause different

Table 2.10: Magnitude and Radius of 1996 TO_{66}

UT	Filter	magnitude	M(1,1)	Radius (km)	Reference
1997 Aug. 27/28	V_B	21.84 ±0.06	5.28	300	Hainaut *et al.* (2000)
1997 Oct. 3/4/6	V_H	21.38 ±0.05	4.75	380	Romanishin & Tegler (1999)
1997 Sept. 23/24	V_J	21.40 ±0.03	4.84[a]	359[a]	Jewitt & Luu (1998)
1999 Nov. 14	V_B	21.61 ±0.01	5.02	337	this work
1999 Dec. 12	V_B	21.63 ±0.01	5.01	339	this work
1997 Sept. 23/24	R_{KC}	21.08 ±0.05	4.52	325[a]	Jewitt & Luu (1998)
1997 Oct. 21/22/23/24/25	R_B	21.15 ±0.05	4.59	326	Hainaut *et al.* (2000)
1998 Sept. 26/27/28	R_{KC}	21.05 ±0.05	4.48	340	Hainaut *et al.* (2000)
1999 Nov. 14	R_B	21.22 ±0.01	4.62	314	this work
1999 Dec. 12	R_B	21.29 ±0.01	4.67	309	this work

Note: V_B and R_B refer to the Bessel filters, V_H refer to the Harris filter, V_J to that in Johnson system, R_{KC} to that in the Kron-Cousin system; M(1,1) is the corresponding absolute magnitude at 1AU.

[a] : Not shown in their paper but calculated in same way as this work.

results in Table 2.10.

Radial profile

The radial profiles of 1996 TO_{66} and of reference stars were obtained from the same 4 sets (V and R for November and December each) of the composite images to search for cometary coma around the object. First, composite images were produced by alignment and stacking of the frames both on the TNO and on stars. Then, the star composite images were normalized to the same intensity as 1996 TO_{66}, providing a Point Spread Function (PSF) for comparison. Finally, the profile was obtained by computing the average flux in annuli 1/2 pixel wide centered on the objects (separately for the TNO and the stars).

We examined 4 composite images to see the difference between the profile of 1996 TO_{66} and the PSF stars. We found no difference between these profiles: (*see* Figure. 2.12) the profile of the TNO perfectly matches that of the PSF, down to the 29 mag/sq.arcsec level, at which the former profile is dominated by noise. We conclude that no coma is visible down to that level. Therefore, if the change of the lightcurve reported by Hainaut *et al.* was caused by a cometary outburst, any remnant coma if present at the time of our observations must have been fainter than the given limit. This is in agreement with the predictions made by Brown & Luu (1998) for the visibility of an outburst coma.

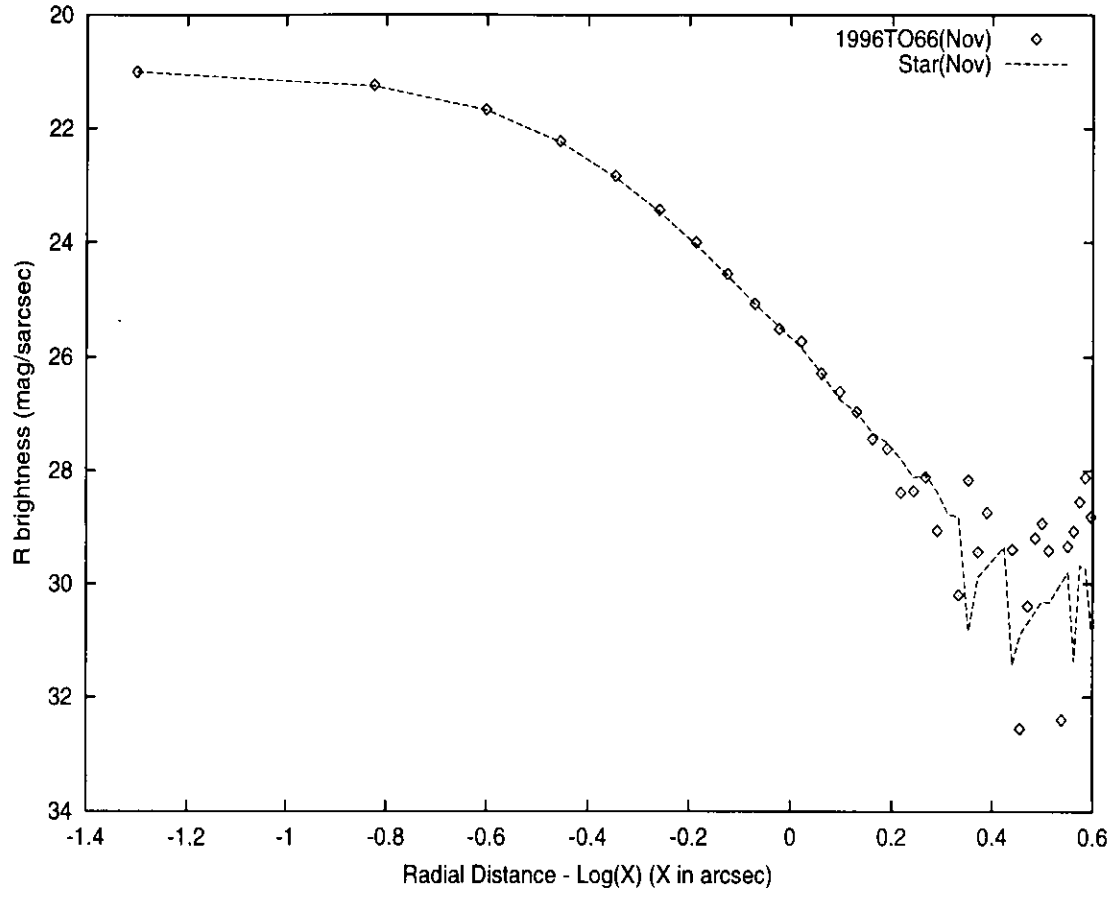

Figure 2.12: Comparison of the radial brightness profile of 1996 TO_{66} (open symbols) and reference stars (dashed line) in our 18 exposures composite image in R. The 1996 TO_{66} profile perfectly matches that of the PSF star.

Lightcurve

The photometric measurements of 1996 TO_{66} for the V and R filters are listed in Table. 2.2.3 and Table. 2.12, respectively. Here, the given error refers to the errors of the aperture photometry measurement. Figure. 2.13 displays the lightcurve of the object in V and R over rotation phase. For planning the measurements, we used the rotation period 6.25 hrs given by Hainaut *et al.* (2000). and obtained a complete coverage of the rotation period through our two observing windows at the VLT.

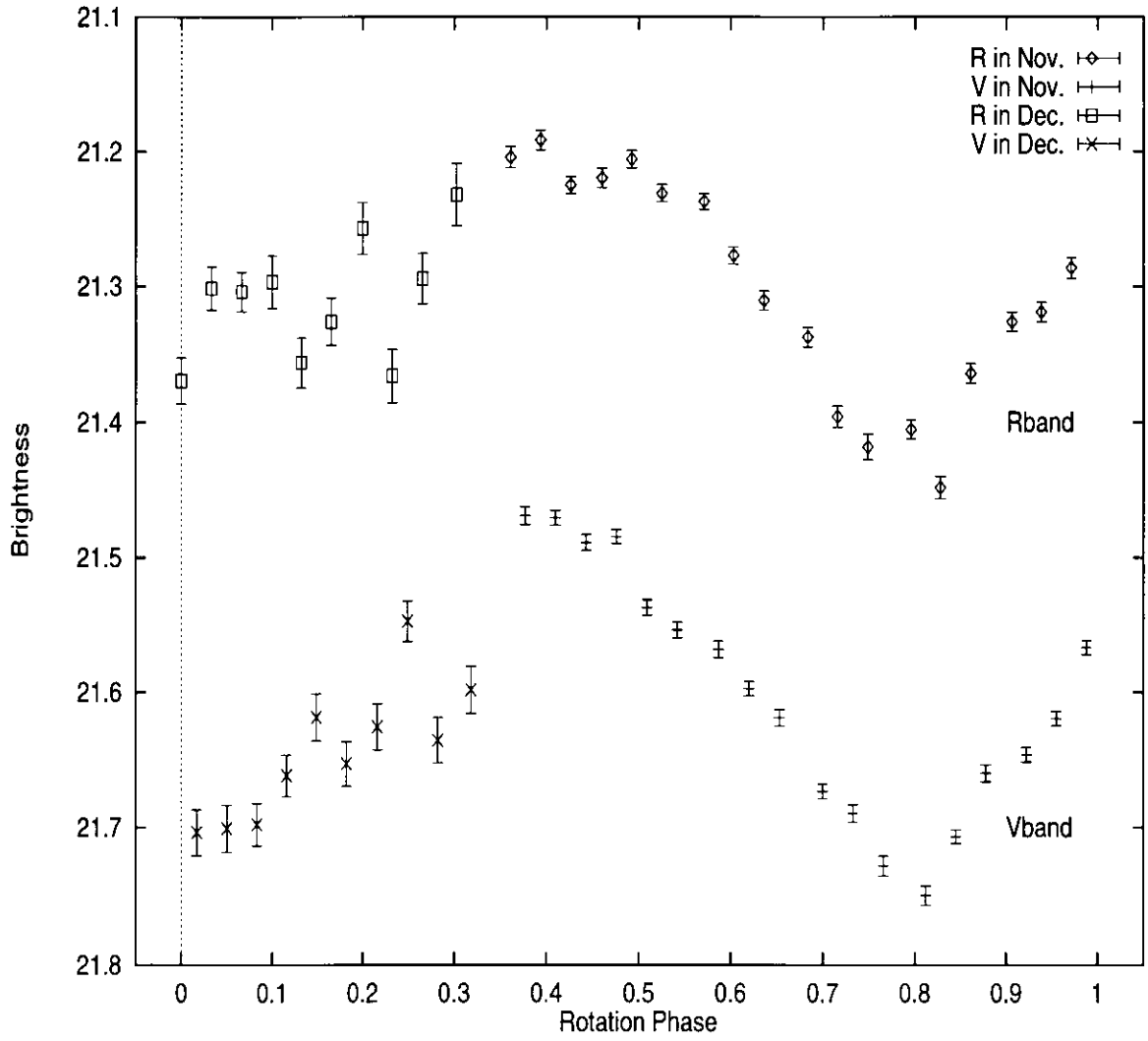

Figure 2.13: Phased lightcurve of 1996 TO_{66}, folded with 6.25h period.

Our result confirms the single peak lightcurve as seen in September, 1998 (Hainaut *et al.*, 2000). The peak-to-peak amplitude is 0.21 mag. This amplitude compares to

Table 2.11: V magnitude of 1996 TO_{66}

UT	Band	Magnitude
1999 Nov 14 00h 32m 49s	V	21.469 ±0.007
1999 Nov 14 00h 45m 11s	V	21.470 ±0.006
1999 Nov 14 00h 57m 38s	V	21.489 ±0.006
1999 Nov 14 01h 09m 56s	V	21.485 ±0.005
1999 Nov 14 01h 22m 22s	V	21.537 ±0.006
1999 Nov 14 01h 34m 43s	V	21.554 ±0.006
1999 Nov 14 01h 51m 33s	V	21.568 ±0.006
1999 Nov 14 02h 03m 55s	V	21.597 ±0.005
1999 Nov 14 02h 16m 21s	V	21.618 ±0.006
1999 Nov 14 02h 33m 45s	V	21.674 ±0.005
1999 Nov 14 02h 46m 05s	V	21.690 ±0.006
1999 Nov 14 02h 58m 32s	V	21.728 ±0.007
1999 Nov 14 03h 15m 47s	V	21.749 ±0.007
1999 Nov 14 03h 28m 10s	V	21.707 ±0.005
1999 Nov 14 03h 40m 35s	V	21.660 ±0.006
1999 Nov 14 03h 57m 09s	V	21.647 ±0.005
1999 Nov 14 04h 09m 31s	V	21.620 ±0.005
1999 Nov 14 04h 21m 53s	V	21.569 ±0.005
1999 Dec 12 01h 32m 49s	V	21.704 ±0.017
1999 Dec 12 01h 45m 15s	V	21.701 ±0.017
1999 Dec 12 01h 57m 43s	V	21.698 ±0.016
1999 Dec 12 02h 09m 58s	V	21.662 ±0.015
1999 Dec 12 02h 22m 23s	V	21.619 ±0.017
1999 Dec 12 02h 34m 48s	V	21.653 ±0.017
1999 Dec 12 02h 47m 28s	V	21.626 ±0.017
1999 Dec 12 02h 59m 52s	V	21.547 ±0.015
1999 Dec 12 03h 12m 16s	V	21.636 ±0.017
1999 Dec 12 03h 25m 52s	V	21.598 ±0.018

V magnitude is corrected by differential photometry with comparison stars. The table lists the date and mid exposure time, the filter, the TNO filter brightness and its photometric uncertainty.

Table 2.12: R magnitude of 1996 TO_{66}.

UT	Band	Magnitude
1999 Nov 14 00h 26m 52s	R	21.204 ±0.008
1999 Nov 14 00h 38m 56s	R	21.191 ±0.007
1999 Nov 14 00h 51m 18s	R	21.224 ±0.006
1999 Nov 14 01h 03m 58s	R	21.220 ±0.007
1999 Nov 14 01h 16m 04s	R	21.256 ±0.007
1999 Nov 14 01h 28m 27s	R	21.231 ±0.006
1999 Nov 14 01h 45m 35s	R	21.237 ±0.006
1999 Nov 14 01h 57m 40s	R	21.277 ±0.006
1999 Nov 14 02h 10m 04s	R	21.310 ±0.007
1999 Nov 14 02h 27m 48s	R	21.347 ±0.007
1999 Nov 14 02h 39m 51s	R	21.400 ±0.008
1999 Nov 14 02h 52m 14s	R	21.418 ±0.009
1999 Nov 14 03h 09m 50s	R	21.405 ±0.007
1999 Nov 14 03h 21m 52s	R	21.447 ±0.008
1999 Nov 14 03h 34m 17s	R	21.364 ±0.007
1999 Nov 14 03h 51m 11s	R	21.326 ±0.007
1999 Nov 14 04h 03m 15s	R	21.318 ±0.007
1999 Nov 14 04h 15m 36s	R	21.296 ±0.008
1999 Dec 12 01h 26m 24s	R	21.370 ±0.013
1999 Dec 12 01h 38m 54s	R	21.323 ±0.012
1999 Dec 12 01h 51m 24s	R	21.340 ±0.011
1999 Dec 12 02h 04m 00s	R	21.370 ±0.014
1999 Dec 12 02h 16m 06s	R	21.401 ±0.013
1999 Dec 12 02h 28m 32s	R	21.343 ±0.014
1999 Dec 12 02h 41m 29s	R	21.374 ±0.015
1999 Dec 12 02h 53m 34s	R	21.390 ±0.014
1999 Dec 12 03h 05m 59s	R	21.386 ±0.015
1999 Dec 12 03h 19m 53s	R	21.298 ±0.018

Column explanations, *see* Fig. 2.2.3.

(*see* Equation. 2.3) a minimum ratio of large to small axis of 1.21 for an ellipsoidal body (assuming a fully shape-induced variability) or to (*see* Equation. 2.4) an albedo change of a factor of 1.21 (assuming that the variability is solely due to surface reflectivity).

The time variation of $(V-R)$ colour is shown in Fig. 2.14. In order to decrease the data scattering, a sliding average of three successive data points were taken for the December data, and of two data points for the November data. Compared to the solar colour $(V-R)_{\odot} = 0.36$, $(V-R)$ of 1996 TO_{66} is - on the average - neutral over the whole rotation phase. This is in agreement with earlier non-phase-resolved photometry and optical low dispersion spectroscopy (Boehnhardt *et al.*, 2001). A small bump around 0.4 rotation phase in the (V-R) colour of 1996TO66 display a change in the colour gradient of the surface material.

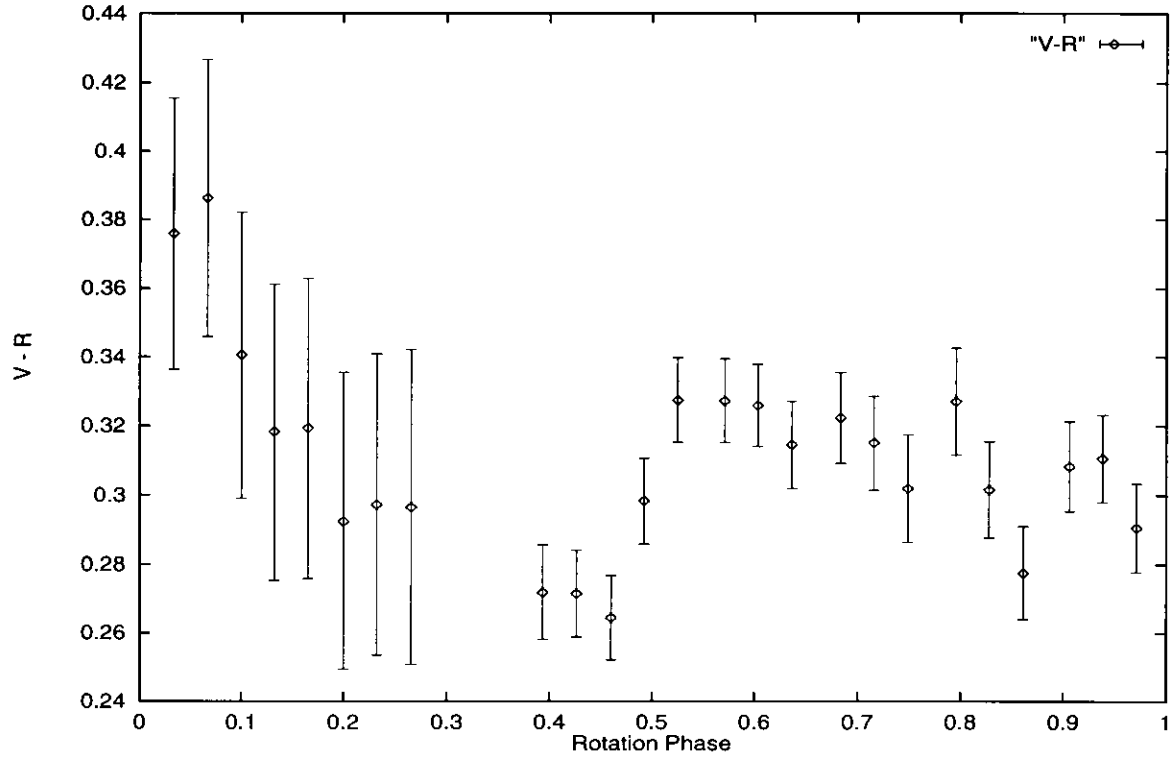

Figure 2.14: Phased V–R curve of 1996 TO_{66}, folded with 6.25h period.

2.2.4 Discussion

Size

The size of 1996 TO_{66} determined from our most recent photometry assuming an albedo of 0.04 is in the expected range and confirms that this TNO is among the largest objects found so far. Compared with other Kuiper Belt relatives, the derived radius is a quarter that of Triton (1353 km) and Pluto (~1200 km), half that of Charon (~600 km), but 2 times bigger than Nereid (170 km).

Lightcurve

Even though we can not improve the rotation period of 1996 TO_{66} than published by Hainaut *et al.* (2000), the phasing of the two parts of the new light curves gives quite good results when using the period of 6.25 h. Therefore, we believe that the combined lightcurve of Nov./Dec. 1999 is intrinsically consistent. The number of rotation cycles in between our two observing runs is 107. The error in the rotation period of the object cannot exceed 0.06h which is however not as accurately determined as in Hainaut *et al.*

There are some lightcurve results of other TNOs published so far (*see* Table. 2.13). The one for 1996 TO_{66} appears to be the most accurate one. The typical rotation periods of a few hours may be a selection effect since considering the monitoring approach for the objects short periods are favored for the detection just because the observing intervals for most objects are not long enough to conclude on rotation periods of one or several days.

We will now summarize the lightcurve observations published and discuss them.

1993 SC: William *et al.* (1995) by whom the object was discovered, reported a 7.7129 hours periodic pattern in this object with the brightness variations of over half a magnitude in R band (11 data points measured over 123.4 h). This period corresponds to a 15.43 hours rotation period and a ratio of 1.6 : 1 for the major to minor axis (assuming the amplitude being due to shape, no albedo variation). On the other hand, Davies *et al.* (1997) derived almost constant brightness of 1993 SC from the differential photometry with 33 data points during 94.3 h in R using a same telescope as William *et al.* The modulation of the lightcurve was less than ~0.1 magnitude. Tegler and Romanishin (1997) also obtained negative results for the variability of 1993 SC using 4 data points in V (71.7 h) and R (72.4 h), respectively. They concluded that a lightcurve variation of 0.5 magnitude was not supported by their data and there was no identification of its period. In addition to this measurements, Romanishin and Tegler (1999) reported the upper limit of brightness variation as 0.12 mag.

Table 2.13: Lightcurve periods and brightness variation amplitudes of TNOs

Objects	D (km)	Δm (mag)	ϵ, θ	P (hours)	Band	Telescope	n	Reference
1993 SC	320	0.5	1.58	7.7	R	INT2.5m[a]	11	William *et al.* (1995)
		≤ 0.1			R	INT2.5m[b]	33	Davies *et al.* (1997)
	240	≤ 0.04			V, R	Bok2.3m[c]	4	Tegler & Romanishin (1997)
	230	≤ 0.12			V	Bok2.3m[c]	8	Romanishin & Tegler (1999)
1994 TB	166	0.34	1.37		$V, R, +$	Bok2.3m[c]	12	Romanishin & Tegler (1999)
	161	0.26	1.27	6.0, 7.0	V, R	Bok2.3m[c]	12	Romanishin & Tegler (1999)
1994 VK_8		0.5	1.58		R	INT2.5m[a]	37	Collander- Brown *et al.* (1999)
	210	0.42	1.47	7.8,8.6,9.4,10.4	V, R	Bok2.3m[c]	15	Romanishin & Tegler (1999)
1995 QY_9	160	0.60	1.74	7	V	Bok2.3m[c]	11	Romanishin & Tegler (1999)
1996 TL_{66}		≤ 0.05			V		6 hr	Luu & Jewitt (1998)
	560	≤ 0.06			V	Bok2.3m[c]	25	Romanishin & Tegler (1999)
1996 TP_{66}		—			R	INT2.5m[a]	29	Collander-Brown *et al.* (1999)
	220	≤ 0.12			V	Bok2.3m[c]	16	Romanishin & Tegler (1999)
1996 TQ_{66}	200	≤ 0.12			V	Bok2.3m[c]	10	Romanishin & Tegler (1999)
1996 TS_{66}	340	≤ 0.12			V	Bok2.3m[c]	7	Romanishin & Tegler (1999)
1997 CQ_{29}	110	≥ 0.38			V	VLT8.2m[c]	12	Boehnhardt (Priv. Comm.)
1997 CS_{29}	530	≤ 0.22			V	Bok2.3m[c]	12	Romanishin & Tegler (1999)
		~ 0.2			R	CA3.5m[d]	9	Boehnhardt (Priv. comm.)
1998 WH_{24}		~ 0.1			R	CA3.5m[d]	9	Boehnhardt (Priv. comm.)
1996 TO_{66}	760	≤ 0.10			V	Bok2.3m[c]	13	Romanishin & Tegler (1999)
	602	0.12	1.12	6.25	V	NTT3.5m[e]	12	Hainaut *et al.* (2000)
	652	0.12	1.12	6.25	R	NTT3.5m[f]	27	Hainaut *et al.* (2000)
	682	0.33	1.36	6.25	R	UH2.2m[g]	55	Hainaut *et al.* (2000)
	662	0.28	1.29	6.25	V	VLT8.2m[h]	28	this work
	620	0.21	1.21	6.25	R	VLT8.2m[h]	28	this work

Notes: D = Diameter,

Δm = Amplitude,

ϵ, θ = minimum ratio of the large to small body axis in case of shape induced variability (*see* equation 2.3)and minimum ratio of the surface albedos in case of surface reflectivity induced variability (*see* equation 2.4)

P = period

n = Number of images,

a: INT2.5m+PrimeCam, b: INT2.5m+TEK3, c: Steward Observatory Bok2.3m (direct), d: Calar Alto observatory 3.5m+MOSCA, e: NTT3.5m+SuSI, f: NTT3.5m+EMMI, g: University of Hawaii 2.2m (direct), h: VLT8.2m+FORS1

1994 TB: Romanishin and Tegler (1999) reported on brightness variation for 1994 TB. They analyzed 2 × 12 data points (~70 and 5 h coverage) taken in V and R filters and compiled as an R band lightcurve by assuming a constant $(V - R)$ colour shift for the object. At the end, they found 2 possible lightcurve periods, which match the data almost equally well, 3.0 and 3.5 h. The axis ratio for shape-induced variability would be around 1.3.

1994 VK_8: Romanishin and Tegler also reported 4 possible lightcurve periods of 1994 VK_8 and an amplitude of 0.42 mag (15 data points in V and R during ~50 h, using the same colour correction technique). Collander-Brown *et al.* (1999) examined the periodicity of 1994 VK_8 as well using a chi-squared method on 37 data points during 28.3 h, and found the signal variation is most likely not due to the object but may be intrinsic to the data (reference star and TNO varied with same periodicity). Interestingly, the data periodicity of 4.75 h seen by Collander-Brown *et al.* is similar to the 4 periods given by Romanishin and Tegler. The brightness change of about 0.4–0.5 mag would imply either a non-sphericalness or significant variation in its surface reflectivity.

1995 QY_9: Romanishin and Tegler reported 3.3–3.7 h period during ~4 h for 1995 QY_9 with an amplitude of 0.60 mag (11 data points in V and R, using the same colour correction technique).

1996 TL_{66}, 1996 TP_{66}, 1996 TQ_{66}, 1996 TS_{66}: Romanishin and Tegler also gave the upper limits for the variation amplitude of 1996 TL_{66}, 1996 TP_{66}, 1996 TQ_{66}, 1996 TS_{66} (*see* Table. 2.13).

1997 CS_{29}: Romanishin and Tegler gave the the upper limits for 1997 CS_{29} as 0.22 mag (12 data points during discrete 3 nights). From recent measurements, 1997 CS_{29} shows ~0.2 magnitude variation in R with 9 data points during consecutive 3 nights (Boehnhardt and collaborators, private communication).

1998 WH_{24}: Recent R band observations (Boehnhardt and collaborators, private communication) showed a ~0.1 mag brightness variation for 1998 WH_{24} over consecutive 3 nights.

1997 CQ_{29}: Recently Boehnhardt and collaborators (private communication) measured amplitude $\geq$ 0.38 mag difference in the V band brightness in 1997 CQ_{29} during 2 consecutive nights.

1996 TO_{66}: Romanishin and Tegler also gave the upper limit for the brightness variation of 1996 TO_{66} of ≤ 0.10 mag (13 data points during discrete 3 nights). On the other hand, Hainaut *et al.* (2000) reported a 6.25 h lightcurve period and a change in the shape and amplitude of its lightcurve between Sep. 1997 (double-peaked lightcurve, amplitude = 0.12 mag) and Sept. 1998 (single-peaked lightcurve, amplitude = 0.3 mag). They measured 27 data points during 5 consecutive nights for in 1997 and other 55 data points during 3 consecutive nights in 1998. With our new observations, we confirm this rotation period and the single-peaked lightcurve, however with a slightly smaller amplitude = 0.21 in V, 0.28 in R, respectively. The results of Romanishin and Tegler appear to be inconsistent with those of Hainaut *et al* (1998) even though they made the observations during same month in 1997. However, the differences could be in the measurement errors, taking into account of $(V - R)$ variation and rotation phase.

In principle, there are two effects which can cause the variation in brightness with rotation of the body: 1) nonspherical body shape and 2) surface material of different albedo. The lightcurve analysis with available data can allow us to assess the potential limits for such variabilities on the respective simple assumption although it is likely that both effects contribute to the overall lightcurve of a TNO.

Body shape

Assuming that the lightcurves are caused by the nonspherical shape of TNOs, a lower limit for the elongation (ϵ) can be estimated as:

$$\epsilon = a/b \geq 10^{0.4\Delta m} \tag{2.3}$$

where Δm is the amplitude of the TNO lightcurve in magnitude. Table. 2.13 lists the rotation periods and body shape parameters – the minimum axes ratio – obtained according to equation (2.3) and using the available data on the variability of TNOs.

Figure. 2.15, Figure. 2.16 and Figure. 2.17 show samples of the shape of body ellipsoids. For example, an axes ratio of 1.74 is claimed for 1995 QY_9. Assuming an homogeneous body, this would result in a 3 times higher surface gravity at the poles of the short axis than that of the long one. One can expect a trend to measure smaller axis ratios for larger body diameters. In this respect it is noteworthy to mention that the supposedly large objects listed in Table. 2.13 (i.e. the ones above 500km diameter) display relatively small amplitudes and are thus not among the objects which would require large (above

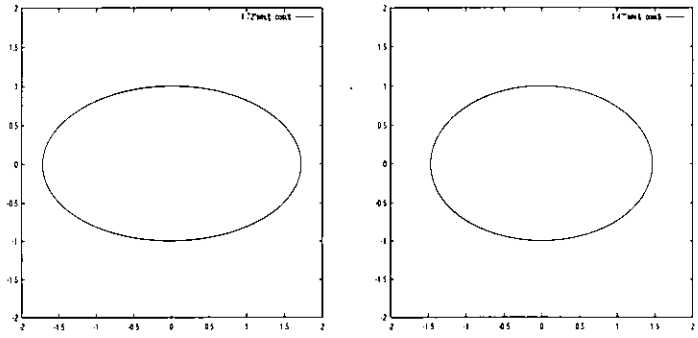

(a) a/b=1.74 (b) a/b=1.47

Figure 2.15: Shape of minor bodies (a/b=1.72, 1.47)

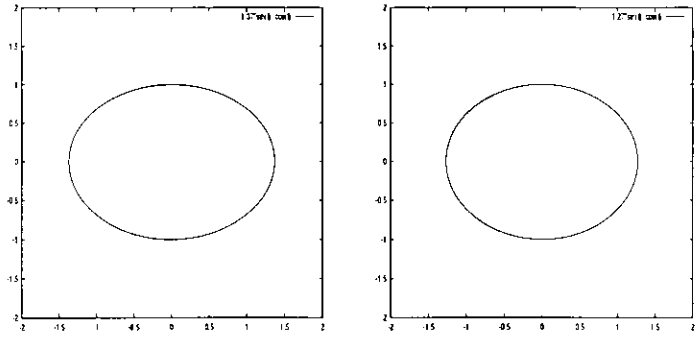

(a) a/b=1.37 (b) a/b=1.27

Figure 2.16: Shape of minor bodies (a/b=1.37, 1.27)

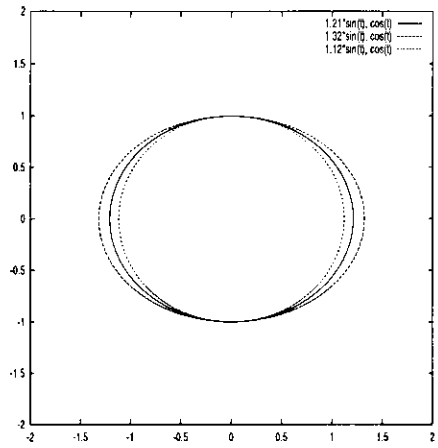

Figure 2.17: Shape of minor bodies (a/b=1996 TO_{66}=1.12,1.21,1.32)

1.3) minimum axis ratio. However, the object sample and the available data on their variability is by far too sparse to allow a firm conclusion.

Albedo

According to Equation (2.2) the ratio of bright to dark albedo for a body of irregular surface reflectivity would be:

$$\theta = p_{\text{bright}}/p_{\text{dark}} \geq 10^{0.4\Delta m} \tag{2.4}$$

where p_{bright} and p_{dark} are the mean albedo of the bright and dark side of the TNO. The interpretation of the observed lightcurve of 1996 TO_{66} in the framework of significant changes of the surface albedo with rotation phase becomes attractive if one could assume an overall low albedo value for this object. On the other side it should be without any net effect on the wavelength dependent reflectivity in the visible wavelength range since on the average the $(V-R)$ colour does not dramatically change over rotation phase. The only exception might be rotation phase of 0.4 where a small bump in the $(V-R)$ colour may indicate a change in the colour gradient of the surface material.

Since pure water ice shows very bluish colour gradient and absorption features in optical and near-IR (e.g. 0.5–2.5 micron spectra – Clark and Lucey 1984), the change of (V-R) around 0.4 rotation phase water ice area is one of the candidate of local blueness. The near-IR spectra of 1996 TO66 in H and K band showed the absorption features near 1.5 and 2.0 micron that are characteristic of water ice (Brown et al. 1999). They reported the intensity of water absorption bands varies with its rotation phase. Phase-resolved

spectroscopy in the near-IR and visible wavelength range would be the adequate tool to address and solve the question of large scale albedo changes over the surface of 1996 TO_{66}.

Patchy surface albedo is found on Pluto (e.g. Buie *et al.* 1997, Young *et al.* 1999, Young *et al.* 2001). Recently, H_2O absorption from Chiron, which had obvious cometary activities before, was detected only after the decline of its activity (Luu *at al.* 2000, Foster *et al.* 1999). Therefore, one might speculate that the surface property of Chiron may be changed by cometary activity. Moreover, two different spectra of 8405 Asbolus (1995 GO) were measured by Kern *et al.* (2000) using HST. This implies that the spectrum of this object has changed within a few hour time interval.

Our data of 1996 TO_{66} can be interpreted by the presence of a bright spot on the surface of this object as described by Hainaut *et al*,. 2000. The anticipated amplitude change of the lightcurve could either be due to a change of the surface of this spot (i.e. the albedo and/or area decreased), or, if the spot was actually a small plume of dust, that the activity causing the plume decreased.

Here, let us explore the hypothesis of cometary activity in TNOs. The equilibrium temperature ($T_{\rm equi}$) of non-sublimating sphere is approximated (Lebofsky and Spencer, 1989) by :

$$T_{\rm equi}{}^4 = \frac{S(1-A)}{R_{\rm h}{}^2\,\sigma\,\eta\,\varepsilon\,\chi} \tag{2.5}$$

where S is the solar constant, $A = p_\lambda\, q$ is the bond albedo (q =0.75 is the bolometric phase integral), σ is the Stefan–Boltzmann constant, $\varepsilon = 0.9$ is the emissivity, $\eta = 0.756$ is the beaming factor, χ ($2 \leq \chi \leq \pi$) expresses effects of fast/slow rotation around its axis. At the solar distance of TNOs, this formula predicts $T_{\rm equi} \simeq 50$ K. Therefore, it may be not unlikely that volatile ices like Methane, Carbon Monoxide and Nitrogen can start sublimating from the surface, if the volatiles are not in clathtrate of water ices, but are directly exposed on the surface of TNOs.

The direct detection of a coma around a TNO may be difficult. A 650km size object at 45.5 AU geocentric distances has a projected diameter of just 0.020 arcsec. The typical FWHM of a reference star in our stacked image is around 0.6 arcsec. Even if the TNO would have 30 $\times$ larger coma than its dimension, it will be difficult to resolve it. Brown and Luu (1998) have modeled dust comae around TNOs considering different body sizes (among them also the case of 1996 TO_{66}). They concluded that comae are rather short-term phenomena (order of a few to 100 days) and dissolve very quickly by escape of the dust to interplanetary space or by impact on the body surface. Even though the authors had impact produced comae in mind, the results should apply in the same way to dust comae from intrinsic activity. The difference however could be that the activity may

produce dust over a longer time interval and/or it may be recurrent.

2.2.5 Summary

The main results of this study are the following:

- The magnitudes of 1996 TO_{66} in V and R are converted into radii of ~330km and ~310km, respectively. These results are in agreement with previous observations.
- Our data are consistent with the 6.25 hr rotation period.
- No resolved coma was detected down to 29 mag/sq.arcsec on a 5400s composite R exposure.
- The $(V - R)$ colour of 1996 TO_{66} has neutral colour over a rotation in general but a small bump around the rotation phase of 0.4 may indicate a change in the colour gradient of the surface material. This supports the inhomogeneous surface material and reflectivity as reported by Brown *et al.* (1999) and Hainaut *et al.* (2000).
- Even though an extended coma is not detected in our images, we can not exclude the existence of cometary activity. The change of the lightcurve amplitude from 1998 to 1999 could be seen as an indication for the presence of such a coma in the seeing disk of 1996 TO_{66}.

These results should be the starting points for a work of surface mapping of TNOs as Pluto.

2.3 Determination Methods of Size and Surface Albedo

In this section, next step to approach the physical properties of the icy minor bodies is described. Because of the faintness of their thermal radiations, even the size and albedo are poorly known so far. Most of current studies to obtain the physical properties are to measure their reflected light of the solar radiation in optical and near-IR. On the other hand, the icy minor bodies emit their blackbody radiation in mid–far IR from themselves. The method to obtain their size and albedo is examined with a bright unusual asteroid which can be a rocky minor body but may be a relative of icy minor bodies in the outer solar system. Finally, the application and feasibility of the determination method are discussed by utilization of possible future instruments such like VLT and ALMA.

Despite all efforts over the past years, sizes and albedo of TNOs, Centaurs and cometary nuclei are only poorly known. For the Centaur Chiron, Campins *et al.* (1994) derived an albedo p_V=0.14 from the mid-IR observation. Altenhoff and Stumpff (1995) supported an albedo p_V=0.13 from millimetre wavelength data at 250GHz. However, these measurements were made when Chiron clearly exhibited a coma which contaminated the nucleus due to additional dust scattering. Therefore, these values should be regarded as an upper limit. Thomas *et al.* (2000) reported the albedos of 2 TNOs, 1993 SC and 1996 TL_{66}, (0.022 and 0.030, respectively) using *ISO* observations. However, the detection levels of those observations were marginal. Recently, Jewitt *et al.* measured the submillimetre continuum radiation of TNO, Varuna (2001 WR_{106}) with JCMT 15m (2001). Their preliminary result for geometric albedo gives a value of 0.07 (+0.03, -0.015). With mid-IR observations, Jewitt and Kalas (1998) derived p_V=0.045 for a inactive Centaur, Chariklo (1997 CU_{26}) as one of the reliable value in 20 μm.

Thermal IR photometry is not an easy technique. In order to confirm the validity of this method, we performed mid-IR observations of a bright target.

2.3.1 Trial for Bright Target: Thermal observations of NEA 1998 SF_{36}

Our original target for work on the determination of size and albedo was a Centaur object, 1997 CU_{26} (Chariklo), when we submit an observing proposal. However, the proper Q-band (20 μm) filter has not been reached to the ESO 3.6m telescope at the observing time since mid-IR instrument TIMMI2 has been just installed. We changed our target and

Table 2.14: Previous results of derived diameters and albedos for Centaurs and TNOs

Object	class	Diameter [km]	Albedo (p_V) [%]	wavelength [μm]	Telescope	References
95P/Chiron	Centaur	$\leq$250	$\geq$5	22.5	IRTF	Lebofsky *et al.* (1984)
	(comet)	$\leq$372	$\geq$2.7	22.5/60	IRTF/IRAS	Sykes *et al.* (1991)
		$\leq$300	$\geq$4	800	JCMT	Jewitt & Luu (1992)
		180	$14\ ^{+6}_{-3}$	10/20	IRTF	Campins *et al.* (1994)
		168	$13\ ^{+4}_{-3}$	1200	IRAM	Altenhoff & Stumpff (1995)
Pholus	Centaur	189	4.4 $\pm$1.3	20	IRTF/UKIRT	Davies *et al.* (1993)
Chariklo	Centaur	302	4.6 $\pm$1.0	20	UKIRT	Jewitt & Kalas (1998)
1993 SC	TNO	164	2.2	90	ISO	Thomas *et al.* (2000)
1996 TL_{66}	TNO	316	3.0	90	ISO	Thomas *et al.* (2000)
Varuna	TNO	900	$7\ ^{+3}_{-1.5}$	850	JCMT	Jewitt *et al.* (2001)

tried to establish a determination method of size and albedo, in our team, adopting it to a bright object in N-band.

Here, we present thermal observations of MUSES-C mission target, 1998 SF_{36}. We measured its mid-IR radiation in N-band (11.9 μm) using the ESO 3.6m telescope with TIMMI2.

The target object, Near-Earth Asteroid (NEA) 1998 SF_{36}, which was discovered by the LINEAR project of MIT Lincoln Laboratory, is the target of the MUSES-C spacecraft mission. MUSES-C is a joint project of the Institute of Space and Astronautical Sciences (ISAS) of Japan and National Aeronautics and Space Administration (NASA) of USA to explore an asteroid, to acquire a sample of the surface material and to return it to Earth. Its launch is scheduled for November or December 2002, arrival at the asteroid in September 2005 and return to the Earth in June of 2007. According to its orbital elements (see Table 2.3.1), NEA 1998 SF_{36}, whose orbital period is about 1.5 years is classified as Apollo, with, semimajor axis $\geq$ 1.0 AU and perihelion distance $\leq$ 1.017 AU.

On March 29, 2001, the object approached within 6.4 million kilometers of the Earth. Extensive ground-based observing were carried out near this close approach time in order to determine the asteroid's approximate size, shape, rotation state, and some surface characteristics (Binzel and Rivkin 2001, Hick *et al.* 2001, Sekiguchi *et al.* 2001, Binzel 2001). The results we present in this paper were obtained in the framework of this ground-based support to MUSES-C.

Table 2.15: Characteristics of Orbital Elements of 1998 SF_{36}

semimajor axis	1.324 (AU)
eccentricity	0.280
inclination	1.723 (degree)
orbital period	1.52 (year)
Orbit type	Apollo

Orbital Elements were published in MPEC 2001-G28.

2.3.2 Thermal Observations with ESO 3.6m + TIMMI2

Thermal observations of 1998 SF_{36} were performed on 2001 March 14.24 UT. N-band (11.9 μm) images were taken with the ESO 3.6m telescope and the TIMMI2 instrument at La Silla Observatory in Chile. TIMMI2, the Thermal Infrared Multi-Mode Instrument 2 (Reimann *et al.*, 2000), has a 240 × 320 pixel AsSiBIB detector. Its image scale is $0.''2$ pixel^{-1} which gives a field of view of $51'' \times 51''$. Individual detector integration time was 16.13 millisecond. For the 4 exposure sets of the asteroid we applied a combination of secondary mirror chopping and telescope nodding as follows: 100 integrations were taken in each of 30 chopping cycles, with an amplitude of $10''$ in North-South direction, then the telescope was moved by $10''$ in East-West and the 30 × 100 chopping exposure sequence was repeated. Hence, the resulting image has 2 positive and 2 negative images of the object (produced by the reduction pipeline which automatically subtracts the pairs of "chopped" images and co-adds all the frames of the whole chopping/nodding sequence). Flatfield correction is not applied to our data since the proper flatfielding method of TIMMI2 image has not yet been established. As a consequence and according to information provided by Käufl, H. U. (priv.comm. 2001), TIMMI2 instrument scientist, we have to consider an error of up to 10 % for the photometry due to lack of flatfield correction of our data.

1998 SF_{36} was visible on the 3.6 m guiding camera, therefore, the telescope could be guided directly on the object. Two exposures of 1998 SF_{36} were obtained with a total integration time of 193.56 s. The infrared standard star HD 47105, whose N-band (12 μm) flux is 5.04 Jy, was observed at higher air mass (1.70) and lower air mass (1.48) than 1998 SF_{36} (air mass, 1.5–1.6). The observing conditions are listed on Table 2.9. From the resulting frame, two positives and two negatives $\times(-1)$ are shifted and stacked resulting in one positive image of 1998 SF_{36}. Figure 2.20 shows the N-band image of 1998 SF_{36} surrounded by the 4 fainter positive ghosts at each corner and 4 fainter negative ghosts in the middle of each side. These ghosts result from the image processing described above.

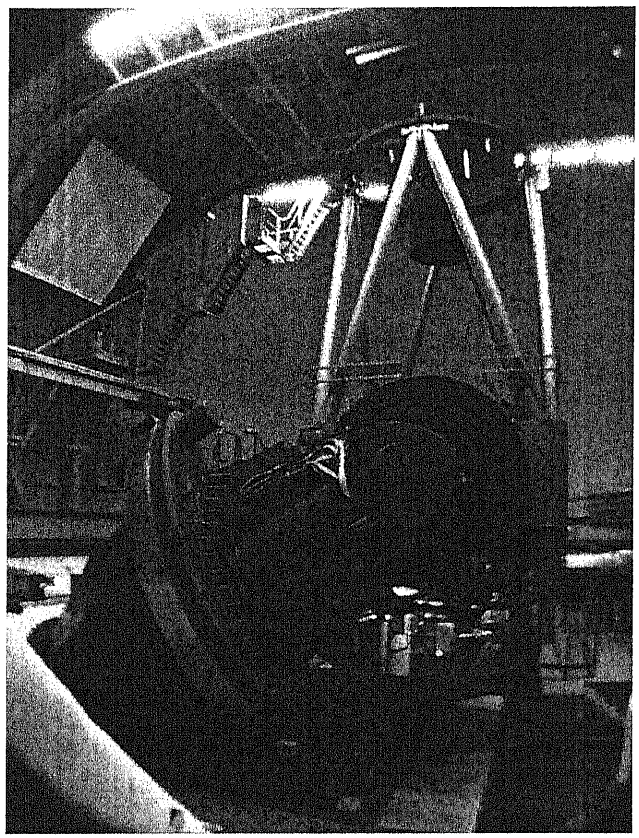

Figure 2.18: ESO 3.6 m Telescope in La Silla Observatory in Chile

Table 2.16: Observing Geometry and Conditions for 1998 SF_{36}

Date (UT)	start–end (UT)	R_h [a] (AU)	Δ [b] (AU)	Phase Angle (deg)	Air mass	Sky
14 Mar. 2001	05:39–06:01	1.0592	0.073920	27.532°	1.54–1.62	photometric

[a] R_h is the heliocentric distance

[b] Δ is the geocentric distance

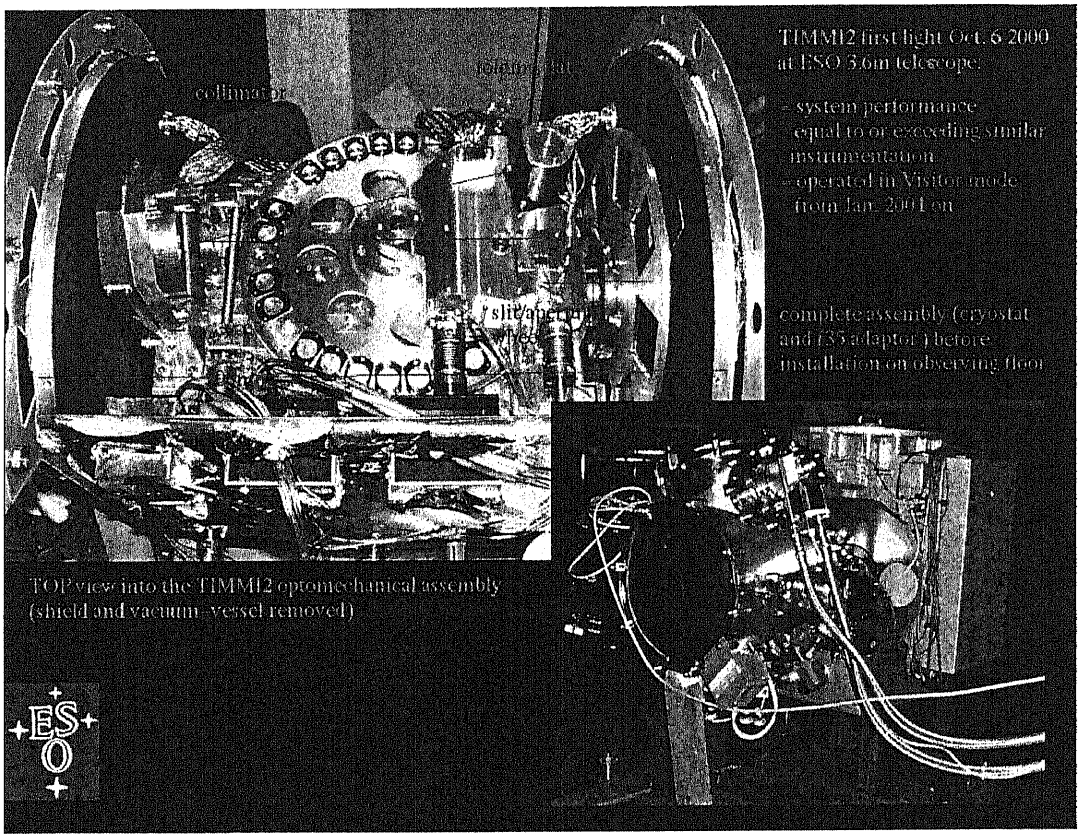

Figure 2.19: TIMMI2 (Thermal Infrared Multi-Mode Instrument 2) attached to ESO 3.6 m Telescope in La Silla Observatory in Chile

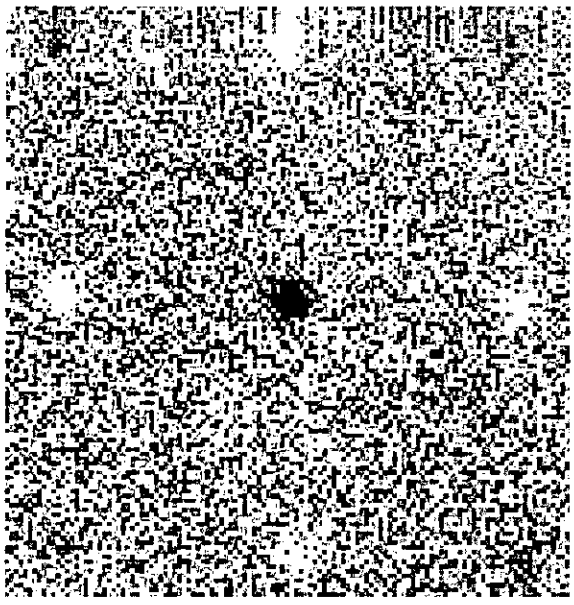

Figure 2.20: N-band (11.9 μm) image of NEA 1998 SF_{36} on March 14, 2001. Chopping and nodding amplitude are 10.″0. North is to the top, and west is toward the right.

2.3.3 Determination Method of Size and Albedo

When the observations only in optical wavelengths are available, one must assume the albedo of minor body to determine its diameter (See section 2.2.3). The brightness of minor body in optical wavelength is a product of the cross-section and albedo. To measure the size of minor body without the assumption of its albedo, it is necessary to measure its thermal radiation. With two independent measurements in optical and thermal-IR, one can determine two parameters simultaneously.

Here, the determination method of size and albedo is described.

The bond albedo A and geometric albedo are related by

$$A = p\,q \tag{2.6}$$

$$\simeq p_V\,q, \tag{2.7}$$

where p and p_V are the bolometric geometric albedo and the geometric albedo in V-band, respectively. q is the bolometric phase integral.

In the H-G system as described by Bowell *et al.* (1989), q is derived from the slope parameter G, via

$$q = 0.290 + 0.684\,G, \tag{2.8}$$

As G is unknown for 1998 SF_{36}, we assumed it to be the standard IRAS value for asteroids,

i.e. $G = 0.15$ (Tedesco, 1986).

Using the absolute magnitude $H = 19.1$ (A. U. Tomatic, 2001) which corresponds to V magnitude at 0° phase angle and heliocentric and geocentric distance of 1 AU, the geometric albedo p_V and the diameter D [km] of asteroid are related by (e.g., Fowler and Chillemi, 1986). It should noted that H is not a H-band magnitude, but an absolute magnitude in V-band among asteroid sciences.

$$\log_{10} D = 3.1236 - 0.2H - 0.5 \log_{10}(p_V), \tag{2.9}$$

The curve defined by Equation (2.9) is shown in Figure 2.21.

On the other side, the thermal flux density of mid-IR radiation from asteroid is given by

$$S_\nu = \pi \varepsilon \, (\frac{r_N}{\Delta})^2 \, B_\nu(T), \tag{2.10}$$

where r_N is the radius of 1998 SF_{36} [m], $\varepsilon = 0.9$ (Lebofsky *et al.*, 1986) is the infrared emissivity and Δ is the geocentric distance [m] and $B_\nu(T)$ is the Planck function for surface effective temperature T [K].

$$B_\nu(T) = \frac{2\, h\nu^3}{c^2} \Big[\exp(\frac{h\nu}{kT}) - 1\Big]^{-1} \tag{2.11}$$

The effective temperature of 1998 SF_{36} is determined by the energy balance at the surface of the asteroid (Lebofsky and Spencer, 1989).

$$\pi \, {r_N}^2 \, (1 - A) \, \frac{S_\odot}{{R_h}^2} = \eta \, \varepsilon \, \sigma \, {r_N}^2 \int_{-\pi}^{\pi} \int_{-\frac{\pi}{2}}^{\frac{\pi}{2}} \Big\{ T^4(\theta, \phi) \, \cos\phi \Big\} d\phi \, d\theta \tag{2.12}$$

where $T(\theta, \phi)$ is the model temperature of spherical minor body at longitude θ and latitude ϕ. This energy balance relation depends on several unknown parameters including, the albedo, emissivity, heat conductivity of surface material, the spin period and the orientation of the spin pole with respect to the Sun. Because of these unknowns, we are not able to derive exactly the temperature distribution on its surface. However, to first level of approximation, the effective temperature ($T_{\rm eff}$) of non-sublimating sphere is given by

$$T_{\rm eff} = \Big[\frac{S_\odot \, (1 - A)}{{R_h}^2 \, \sigma \, \varepsilon \, \eta \, \chi} \Big]^{\frac{1}{4}}, \tag{2.13}$$

where $S_\odot = 1365$ W m^{-2} is the solar constant and $\sigma = 5.671$ W m^{-2} K^{-4} is the Stefan-Boltzmann constant. R_h is the heliocentric distance [AU]. The correction factor η is called "beaming factor". It adjusts the surface temperature to compensate for the angular distribution of the thermal emission and, usually, is set to $\eta = 0.756$ for main belt asteroids (Lebofsky *et al.* 1986). Here, we adopt $\eta = 1.2$ which was derived for NEAs by Harris.

(1998). They proposed this value when observations at only one or two wavelengths are available. In this case, χ which expresses effects of rotation around its axis, is taken as 2 for the Standard Thermal Model (Jewitt & Kalas, 1998) since the rotation of 1998 SF_{36} is not fast ($P_{\rm rot}$ ~12 hr, Abe, priv.comm.).

2.3.4 Results – Size and Albedo

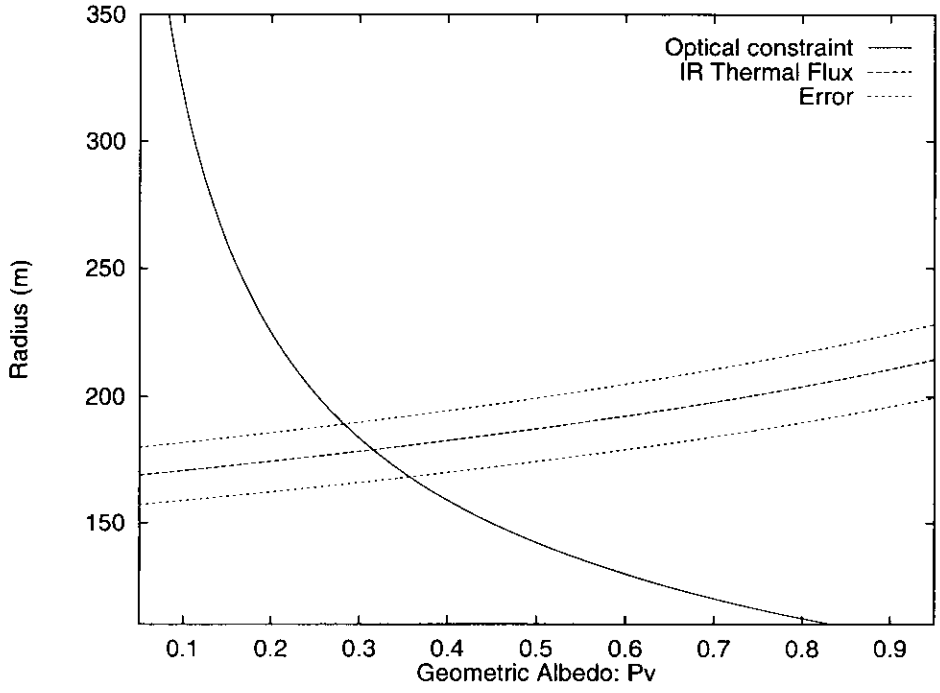

Figure 2.21: Constraints on the albedo and radius of 1998 SF_{36} from thermal infrared observations and optical absolute magnitude.

Mid-IR radiation of 1998 SF_{36} and of the standard star were measured from the N-band images with an aperture photometry method. The PSF-FWHM measured on 1998 SF_{36} and standard star was 0.″84. Three times FWHM was taken as the aperture diameter and measured flux of 1998 SF_{36} was 0.256 ±0.043 Jy. The given error refers to the errors of the photometry measurement including the uncertainty from basic reductions. Then, we adopted an average IR phase coefficient $\beta_{\rm E} = 0.01$ mag deg^{-1} determined by Matson (1971) who found for asteroids $\beta_{\rm E}$ in the ranged from 0.0005 to 0.017 mag deg^{-1}. This value is generally considered to be valid for phase angles $\leq 30°$ (Morrison, 1977).

Figure 2.21 shows the diameter versus the geometric albedo relationships defined by optical constraint of Equation (2.9) and thermal-IR constraint of Equation (2.10). The in-

tersection of those curves gives the best estimate of the radius, $r_N = 178$ (+13/−14) m, and the geometric albedo, $p_V = 0.29$ (+0.05/−0.04) of 1998 SF_{36}. These result are consistent with the preliminary classification of 1998 SF_{36}: Binzel and Rivkin (2001) reported S-type reflectance from optical spectroscopy at 0.5–1.0 μm. Hick *et al.* (2001) reported that the object exhibits a spectrum dominated by olivine due to deep 1-micron absorption feature from spectroscopy at 0.35–1.0 μm. Therefore, they suggested type Q, R or S classification. Q-type, R-type and S-type have relatively high albedo (Tholen and Barucci, 1989). However, systematic errors from uncertainties in the unknown parameters clearly exceed the presented errors. For instance, if we adopt a traditional value of the beaming parameter for main belt asteroids, $\eta = 0.756$, the derived curves gives $r_N = 147$ (+10/−11) m and $p_V = 0.47$ (+0.07/−0.06), respectively.

In conclusion, despite some model-depending uncertainties, the MUSES-C mission target 1998 SF_{36} has a small radius of 150–300 m and the derived albedo range of 0.2–0.5, is consistent with the spectroscopic classification.

2.3.5 Thermal Observations with New telescopes / Instrument equipments

The geometric albedo of minor bodies in the solar system is one of their most basic parameter. It can be measured by simultaneous photometry of thermal radiation in mid- (or far)-IR and solar reflected light in optical. Unfortunately, for TNOs, Centaurs and cometary nuclei, it is poorly known because of the faintness of these objects. A value of 0.04, which was measured for 1P/Halley by spacecrafts, is usually assumed for size estimations when only optical observations are analyzed. While some observations of other objects support the use of this value, very different albedo are also reported (e.g. 0.13 for 95P/Chiron).

TNOs, Centaurs and SPCs are hypothesized to be candidates of pristine and mostly unaltered planetesimals. Apparently, these three object classes cover a wide range of sizes (from a few 100 km to a few 100m) and they are subject to different environmental conditions which possibly led their surfaces evolve differently and with different time scales. Understanding the basic properties of TNOs, Centaurs and SPCs, the most primitive objects orbiting the Sun at larger distances, and their evolution with time will provide clues on the initial conditions for the Solar System. Measuring their sizes and the albedo is an important step toward the answer of this fundamental problem of planetary sciences.

However, the dimensions of these objects cannot be resolved from Earth. So far, only 1P/Halley was really measured for size and albedo by a spacecraft. Therefore, the only way for determination of their sizes and albedo from ground-based observations is to measure

the total energy balance of the reflected light of Sun and thermally emitted light from the objects as shown above. Depending on the distance of the objects the peak thermal emission falls in the mid-IR to sub-mm wavelength range which makes detection from the ground a challenge. For objects at 5-20 AU the maximum flux lies around 20–1000 μm (see Fig 2.22), i.e. they can be detectable with mid-IR instruments if they are bright/large enough. Compared to the thermal band, the reflected light is easily measurable through broadband photometry in the visible wavelength range.

TNOs Study toward Next Step

At present, new telescopes and new instruments for mid-IR and submillimetre wavelength rage have been built and are being built. We start considering determination of the most basic parameters for the faint distant minor bodies. Using mid-IR instruments, for example, TIMMI2 of the ESO-3.6m, VISIR of the ESO-VLT, COMICS of the Subaru and so on., it became to observe nearer objects from near Earth region to giant planets region i.e. near Earth asteroids (NEAs), main belt asteroids, Trojan asteroids and Centaurs.

The feasibility of thermal observation of minor bodies with new instruments was estimated with the Standard Thermal Model (See section 2.3.1). As a representation of NEAs, 1998 SF_{36} is adopted. 1997 CU_{26} (Chariklo) for a Centaur, 2000 WR_{106} (Varuna) for TNO are adopted.

N-band is an atmospheric window around 10 μm, Q-band is around 20 μm.

Figure 2.22 shows the estimated thermal flux over full thermal-IR wavelength range (from a few μm to a few mm) and the sensitivity of each instrument. Their sensitivities are expressed as 10 σ detectability in hour. The effective wavelength for observations depends on the characteristics of efficiency of each instrument and depends on the effective surface temperature of each object.

Table 2.17: Representative objects and their effective wavelength for thermal observation.

Representative Object	Dynamical Class	Effective Wavelength
1998 SF_{36}	Near Earth Asteroid (NEA)	N-band & Q-band
1997 CU_{26} (Chariklo)	Centaur	Q-band & sub-mm
2000 WR_{106} (Varuna)	Trans-Neptunian Object (TNO)	sub-mm

Near Earth objects have enough flux in N-band. It is possible to observe them with mid-IR instruments (for instance, the ESO 3.6m + TIMMI2,

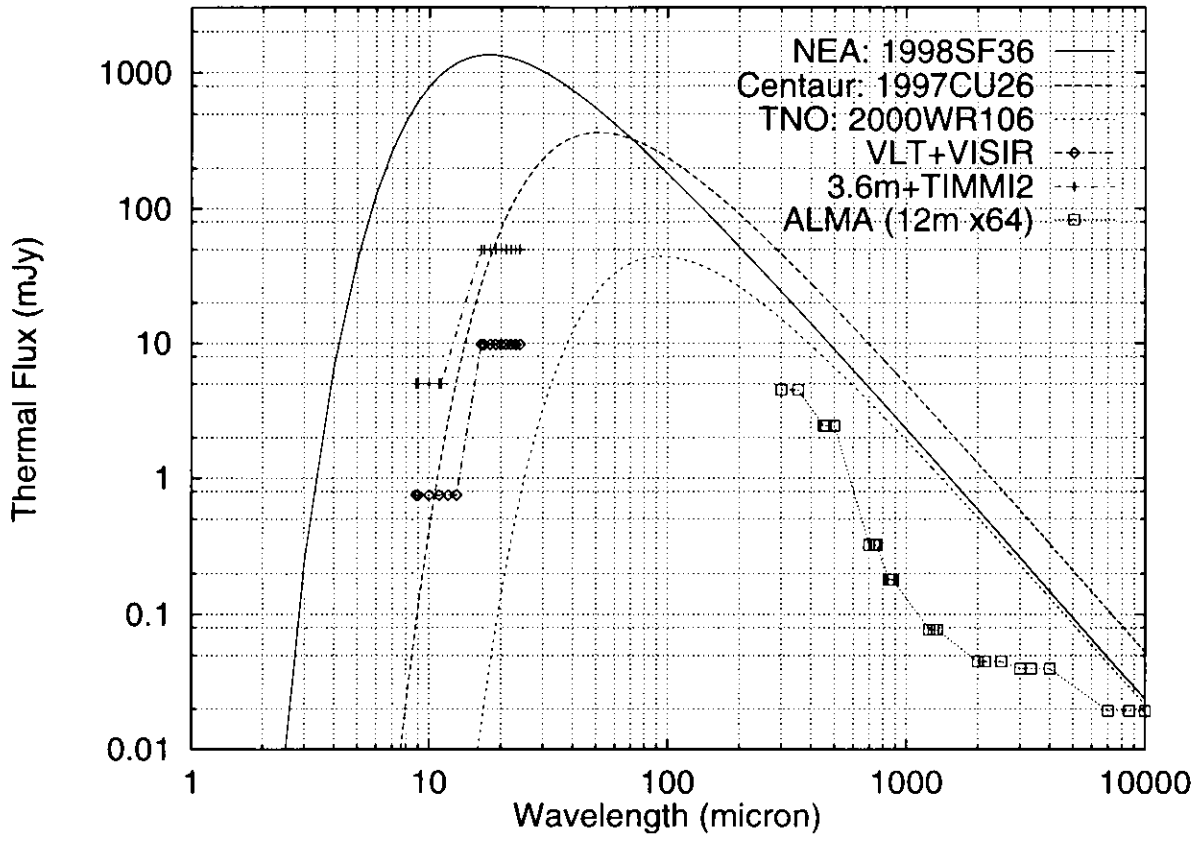

Figure 2.22: Thermal flux vs S/N=10, 1 hour sensitivity

see http://www.ls.eso.org/lasilla/Telescopes/360cat/timmi/html/performance.html). For Centaur objects, Q-band observations with current mid-IR instruments are also possible. Even the most powerful ground-based instruments like the ESO-VLT + VISIR, however, it is impossible to detect TNOs in N-band nor Q-band (for detailed information see the ESO web page http://www.eso.org/instruments/visir/) (Note: Sensitivity of Subaru + COMICS is thought to be comparable to the ESO-VLT + VISIR).

Here, let us consider a future large project, the Atacama Large Millimeter Array. The Atacama Large Millimeter Array (ALMA) is the name for the merger of a number of major millimeter array projects into one global project: the European Large Southern Array (LSA), the U.S. Millimeter Array (MMA), and the Japanese Large Millimeter and Submillimetre Array (LMSA). This project will be the largest ground-based astronomy project of the next decade.

The sensitivity of ALMA is not known yet. Now, using expected sensitivity (see, http://www.mma.nrao.edu/info/sensitivities/index.html), ALMA's great powerful sensitivities would allow us to establish a real size distribution of observable TNOs without the assumption of surface albedo. This will give a strong boundary condition on the theory of the solar system formation.

Chapter 3

Summary

In order to extend the knowledge and to reveal the characteristics of icy minor bodies in the outer solar system, various photometric observations in wide wavelength were performed using large telescopes.

- **Visible and near-IR photometry**
  Visible ($BVRI$) and near-IR (JHK_s) broadband photometry and visible low-dispersion spectroscopy of Trans-Neptunian Objects (TNOs) and Centaurs are carried out in order to characterize their reflectance properties.

  - On the contrary to former result which showed the existence of 2 distinct populations of their colours, the continuous colour distribution from solar to reddened colour was obtained.
  - The correlation between absolute magnitude and the $V - I$ colours was not supported.
  - Further observational works for distant minor bodies are still strongly required to establish a classification such as a taxonomy of main belt asteroids.

- **Time-resolved bi-colour photometry**
  Time-resolved photometry together with high spatial resolution imagings with the ESO VLT 8.2m in V and R-band were performed in order to verify the lightcurve change, to address potential colour variation with rotation phase and to search for the presence of a cometary coma,

  - No resolved coma was detected from TNO 1996 TO_{66} down to 29 mag/sq.arcsec on a 5400s R exposure.

- The $(V - R)$ colour of 1996 TO_{66} has neutral colour over a rotation indicates an inhomogeneous surface material or surface aging. The future work such like surface mapping of TNOs should follow after these observations.

- **Thermal IR photometry**
  The determination method and its feasibility for the most basic parameters, size and albedo of outer minor bodies are discussed. As a trial case, a bright asteroid was analyzed with mid-IR observations.

  - Determination method of size and albedo of icy minor bodies was examined for a bright asteroid and it was confirmed.

Further observations are necessary since the presented results in this paper were not in a final status. This work should be execute continuously to extend the knowledge of icy minor bodies as remnants of pristine objects in the early solar system.

ACKNOWLEDGMENTS

I would like to thank my advisor Dr. Junichi Watanabe of the National Astronomical Observatory (NAO) for sharing his enthusiasm for science and for guiding me during the course of my doctoral thesis. His suggestions sometime brought drastic changes in my study life (e.g. he suggested me to join to the ESO solar system observing team).

This thesis is based on the observations and studies carried out at the European Southern Observatory (ESO), Chile through the ESO Ph.D studentship programme. I am grateful to Dr. Hermann Böhnhardt of ESO for being one of the supervisor of my doctoral study as well as guiding my thesis work. He also gave me a splendid chance to perform observations at the famous and fantastic observatories such the Paranal observatory and the La Silla observatory in Chile. I am thankful to Dr. Olivier Hainaut for providing many helpful methods for the data reduction using his MIDAS program and for his help. I appreciate kind the effort of Dr. Danielle Alloin for making my stay at ESO comfortable and extending my contract with ESO for finishing my work. I had lots of great experiences during stay at ESO and in Chile for 2 years and half. It is a great pleasure to thank all ESO members. Thanks also go to my colleagues, Ph.D-less people at the ESO student office in Chile: Cathy, Michael, Franck, Sebastian, Benoit, Emeric, Emmanuel and new generations i.e. Audrey, Cecil, Dominique, Oliver, Paul, Frederic. Their boundless enthusiasm and inspiration helped keep me interested in this research even through the most frustrating days.

I would also like to express my appreciation to Prof. Hiroshi Kinoshita for taking on the responsibility of the doctoral course at the Graduate University for Advanced Studies. I express my thank to Dr. Nobuharu Ukita and Mr. Hitoshi Hasegawa for their guidance in radio astronomy even though the study of CO emission of Centaur, Chiron in millimeter wavelength was deleted from this thesis after referee cycle. I thank Prof. Toshio Fukushima at NAO, Prof. Tetsuo Yamamoto at Nagoya University and Dr. Motohide Tamura at NAO for their critical suggestions and for referring the thesis. It is a pleasure to thank Dr. Takashi Ito at NAO for helpful discussions. Many thanks also go to my dear students at NAO.

Finally, I would like to thank my parents and Rena for enduring for the long time I spent getting my degree.

Bibliography

[1] A. U. Tomatic, (Minor Planet Center, Smithsonian Astrophysical Observatory), 2000, MPEC. 2000-P19

[2] A. U. Tomatic, (Minor Planet Center, Smithsonian Astrophysical Observatory), 2001, MPEC. 2001-G28

[3] Altenhoff, W. J. and Stumpff, P., 1995, *A&A*, **293**, L41

[4] Barucci, M.A., Doressoundiram, A., Tholen, D., Fulchignoni, M., and Lazzarin, M., 1999a, *Icarus*, **142**, 476

[5] Barucci, M.A., Lazzarin M., Tozzi G.P., 1999b, *AJ*,**117**, 1929

[6] Barucci, M.A., Romon J., Doressoundiram A., Tholen D.J., 2000, *AJ*, **120**, 496

[7] Binzel, R. P., 2001, *IAUCircular*. 7609

[8] Binzel, R. P. and Rivkin, A. S., 2001, IAU*Circular*. 7598

[9] Boehnhardt, H., Tozzi, G.P., Birkle, K., Hainaut, O., Sekiguchi, T., Vair, M., Watanabe, J., Rupprecht, G., and The FORS Instrument Consortium, 2001, *A&A*, *submitted*

[10] Bowell, E., Hapke, B., Domingue, D., Lumme, K., Peltoniemi, J. and Harris, A. W., 1989 In *Asteroids II*, ed. Binzel, R. and Gehrels, T. and Matthews (Tucson: Univ. Arizona Press), 524

[11] Brown, R. H., Cruikshank, D. P. and Pendleton, Y., 1999, *ApJ*, **519**, L101

[12] Brown, W. R. and Luu, J., 1998, *Icarus*, **135**, 415

[13] Buie, M., Young, E.,and Binzel, R., 1997, in *Pluto and Charon*, ed. Stern, A., Tholen, D. (Tucson: Univ. Arizona Press), 269

[14] Bus, S. J., A'Hearn, M. F., Schleicher, D. G., & Bowell, E., 1991, *Science*, **251**, 774

[Clark & Lucey(1984)] Clark, R. N. and Lucey, P. G., 1984, *JGR*, **89**, 6341

[15] Campins, H., Telesco, C. M., Osip, D. J., Rieke, G. H., Rieke, M. J. and Schulz, B., 1994, *AJ*, **108**, 2318

[16] Collander-Brown, S. J., Fitzsimmons, A., Fletcher, E., Irwin, M. J. and Williams, I. P., 1999, *MNRAS* , **308**, 588

[17] Cruikshank D.P., Roush T.L., Bartholomew M.J., Geballe T.R., Pendleton Y.J., White S.M., Bell J.F., Davies J.K., Owen T.C., de Bergh C., Tholen D.J., Bernstein M.P., Brown R.H., Tryka K.A. and Dalle Ore C.M., 1998, *Icarus* **135**, 389

[18] Davies, J. K., McBride, N., and Green, S. F., 1997, *Icarus*, **125**, 61

[19] Davies J.K., Green S., McBride N., Muzzerall E., Tholen D.J., Whiteley R.J., Foster M.J. and Hillier J.K., 2000, *Icarus*, **146**, 253

[20] Dones, L., Levison, H., Duncan, M., and Weissman, P., 2000, AAS/Division of Planetary Sciences Meeting, **32**, 3602

[21] Edgeworth, K. E., 1943, *J.B.A.A.*, **53**, 181

[22] Edgeworth, K. E., 1949, *MNRAS*, **109**, 600

[23] Foster, M. J., Green, S. F., McBride, N. and Davies, J. K., 1999, *Icarus-Note*, **141**, 408

[24] Fowler, J. W. and Chillemi, J. R., 1986, In *IRAS Asteroid and Comet Survey*, ed. Matson, D. L. (JPL: IPAC), 6-1

[25] Giacconi R., Gilmozzi R., Leibundgut B., Renzini, A., Spyromilio J., Tarenghi M., 1999, *A&A*, **343**, L1

[26] Hainaut, O. R., Delahodde, C. E., Boehnhardt, H., Dotto, E., Barucci K. J. Meech, M. A., Bauer, J. M., West, R. M. and Doressoundiram, A., 2000, *A&A*, **356**, 1076

[27] Hainaut, O. R., Meech, K. J., Boehnhardt, H. and West, R. M., 1998, *A&A*, **333**, 746

[28] Harris, A. W., 1998, *Icarus*, 131, 291

[29] Hayashi, C., Nakazawa, K., & Nakagawa, Y., 1985, In *Protostars and Planets II*, ed. Black, D.C. and Matthews, M.S., (Tucson: Univ. Arizona Press), 1100

[30] Hick, M., Weissman, P., Chamberlin, A. and Lowry, S., 2001, *IAUCircular.* 7598

[31] Jewitt, D., Aussel, H., & Evans, A., 2001, *Nature*, **411**, 446

[32] Jewitt, D. and Luu, J., 1989, *AJ*, **97**, 1766

[33] Jewitt, D. & Luu, J., 1993, *Nature*, **362**, 730

[34] Jewitt, D. C. and Luu, J. X., 1998, *AJ*, **115**, 1167

[35] Jewitt, D. and Kalas, P., 1998, *ApJ.L*, **499**, L103

[36] Kern, S. D., McCarthy, D. W., Buie, M. W., Brown, R. H., Campins, H. and Rieke, M., 2000, *ApJ*, **542**, L155

[37] Khare, B. N., Sagan, C., Arakawa, E. T., Suits, F., Callcott, T. A. and Williams, M. W., 1984, *Icarus*, **60**, 127

[38] Kuiper, G., 1951, *In Astrophysics: A total Sympositum*, ed. Hynek, J.A., McGraw-Hill, New York, 357

[39] Landolt, A., 1992, *AJ*, **104**, 340

[40] Lebofsky, L. and Spencer, J., 1989, in *Asteroids II*, ed. Binzel, R. and Gehrels, T. and Matthews, M.S. (Tucson: Univ. Arizona Press), 128

[41] Lebofsky, L. A., Sykes, M. V., Tedesco, E. F., Veeder, G. J., Matson, D. L., Brown, R. H., Gradie, J. C., Feierberg, M. A. and Rudy, R. J., 1986, Icarus, 68, 239

[42] Levison, H. F. and Duncan, M. J., 1997, *Icarus*, **127**, 13

[43] Levison H.F., 2001, IAU Joint Discussion 4, in: Highlights in Astronomy (ed. H. Rickman), in press

[44] Luu, J. and Jewitt, D., 1990, *Icarus*, **86**, 69

[45] Luu, J. X., 1993, *Icarus*, **104**, 138

[46] Luu, J. X. and Jewitt, D. C., 1996a, *AJ*, **111**, 499

[47] Luu, J. X. and Jewitt, D. C., 1996b, *AJ*, **112**, 2310

[48] Luu, J. X. and Jewitt, D. C., 1998, *AJ*, **494**, L117

[49] Luu, J. X., Jewitt, D. C. and Trujillo, C., 2000, *APJL*, **531**, L151

[50] Matson, D. L. 1971, IAU Colloq. 12: Physical Studies of Minor Planets, 45

[51] Meech, K. J. & Belton, M. J. S., 1990, *AJ*, **100**, 1323

[52] Meech, K. J., 2001, private communication

[53] Meeus J., 1998, Astronomical Algorithms, Willmann-Bell Inc., Richmond, USA

[54] Morrison, D., 1977, ApJ, 214, 667

[55] Noll L.S., Luu J., Gilmore D., 2000, *AJ*, **119**, 970

[56] Rabinowitz, D. L., 1997, *Icarus*, **127**, 33

[57] Reimann, H., Linz, H., Wagner, R., Relke, H., Kaeufl, H. U., Dietzsch, E., Sperl, M., & Hron, J., 2000, Proceedings. SPIE, 4008, 1132

[58] Romanishin, W. and Tegler, S. C., 1999, *Nature* , **398**, 129

[59] Romon J., Barucci M.A., Doressoundiram A., 2001, in: Highlights of Astronomy (ed. H. Rickman), PASP conference series, submitted

[60] Russell, H. N., 1916, *AJ*, **43**, 173

[61] Sagan, C., Khare, B. N., and Lewis, J. S., 1984, in *Saturn*, ed. Matthews, M.S. and Gehrels, T., (Tucson: Univ. Arizona Press), 788

[62] Sekiguchi T., Boehnhardt H., Delahodde C.E., Hainaut O., 2001, *A&A*, submitted

[63] Sekiguchi, T., Sterzik, M., Ageorges, N. and Hainaut, O., 2001, IAU *Circular.* 7598

[64] Shul'man L.M., 1972, in: The Motion, Evolution of Orbits, and Origin of Comets (ed. Chebotarev et al.), IAU Symp. **45**, Reidel Dordrecht, 265

[65] Stern, S. A. 1995, *AJ*, **110**, 856

[66] Stern, S. A., 1996, *A&A*, **310**, 999

[67] Tedesco, E. F., 1986, E. F. in *IRAS Asteroid and Comet Survey*, ed. Matson, D. L. (JPL: IPAC), 9-1

[68] Tegler, S. C. and Romanishin, W., 1997, *Icarus*, **126**, 212

[69] Tegler, S. C. and Romanishin, W., 1998, *Nature* **392**, 49

[70] Trujillo C.A., Jewitt D., Luu J., 2000, BAAS 32, 2004

[71] Tholen, D. J. and Barucci, M. A., 1989, In *Asteroids II*, ed. Binzel, R. and Gehrels, T. and Matthews (Tucson: Univ. Arizona Press), 298

[72] Thomas, N., Eggers, S., Ip, W.-H., Lichtenberg, G., Fitzsimmons, A., Jorda, L., Keller, H. U., Williams, I. P., Hahn, G. and Rauer, H., 2000, *ApJ*, **534**, 446

[73] Weissman, P. R. and Levison, H. F., 1997, *APJL*, **488**, L133

[74] Williams, I. P., O'Ceallaigh, D. P., Fitzsimmons, A. and Marsden, B. G., 1995, *Icarus*, **116**, 180

[75] Wyckoff S., 1982, in: Comets (ed. L.L. Wilkening), Univ. Arizona Press, 3

[76] Young, E. F., Galdamez, K., Buie, M. W., Binzel, R. P. and Tholen, D. J., 1999, *AJ*, **117**, 1063

[77] Young, E., Binzel, R. and Crane, K., 2001, *AJ*, **121**, 552